Journal of Petroleum Science and Engineering 203 (2021) 108601

Contents lists available at ScienceDirect

Journal of Petroleum Science and Engineering

journal homepage: http://www.elsevier.com/locate/petrol

Evolution of abnormal pressure in the Paleogene Es_3 formation of the Huimin Depression, Bohai Bay Basin, China

Qiaochu Wang [a,b], Dongxia Chen [a,b,*], Xianzhi Gao [a,b], Fuwei Wang [a,b], Sha Li [a,b], Ziye Tian [a,b], Wenzhi Lei [a,b], Siyuan Chang [a,b], Yi Zou [a,b]

[a] State Key Laboratory of Petroleum Resources and Prospecting, China University of Petroleum (Beijing), Beijing, 102249, China
[b] College of Geosciences, China University of Petroleum (Beijing), Beijing, 102249, China

ARTICLE INFO

Keywords:
Abnormal pressure evolution
Overpressure
Underpressure
Origin
The Huimin Depression

ABSTRACT

The evolution of abnormal pressure is of importance for the analysis of hydrocarbon migration and accumulation processes. However, paleo-pressure reconstruction is still a challenge with great uncertainty. In this study, the PVT simulation method and homogenization temperature-salinity method were used for abnormal pressure evolution analysis in the Huimin Depression, which is characterized by a complex distribution of abnormal pressure, including overpressure, normal pressure and underpressure. The origins of the abnormal pressure conditions were also analyzed to examine the rationality and reliability of paleo-pressure reconstruction by basin modeling and quantitative calculation. The results revealed different evolutionary processes for the paleo-pressure in the Central Deep-Sag Zone (CDSZ) and the Northern Tectonic Uplift Belt (NTUB). In the CDSZ, the abnormal paleo-pressure exhibited a rising stage during the late Oligocene owing to disequilibrium compaction. From the early to middle Miocene, the paleo-pressure decreased to hydrostatic pressure because of the elastic rebound of rocks and temperature reduction. From the late Miocene to middle Pliocene, the paleo-pressure rose again because of the deposition and hydrocarbon generation. From the late Pliocene to the present, the paleo-pressure decreased again owing to the termination of hydrocarbon generation and secondary migration of hydrocarbons. In the NTUB, the paleo-pressure remained hydrostatic without disequilibrium compaction during the late Oligocene, followed by an intense reduction process due to rock elastic rebound and temperature reduction owing to strong tectonic uplift from the early to middle Miocene. From the late Miocene to middle Pliocene, the paleo-pressure rose because of the deposition and hydrocarbon injection from the CDSZ. From the late Pliocene to the present, the termination of hydrocarbon generation, weakening of hydrocarbon injection from the CDSZ, and the gas diffusion led to the decrease of pressure again in the NTUB. This study reveals that the paleo-pressure experienced two rising and two falling stages in the CDSZ and finally is characterized from normal pressure to overpressure. The paleo-pressure in the NTUB experienced one rising and two falling stages and is currently characterized by underpressure. This study provides a new approach for assessing the paleo-pressure evolution based on multiple analytical methods and further contributes to research on hydrocarbon-accumulating dynamics and hydrocarbon-migrating processes.

1. Introduction

Abnormal pressures have been observed in a wide range of petroliferous basins (Magara, 1975; Law and Spencer, 1998). The distribution, origin, and evolution of abnormal pressure is of great importance to hydrocarbon accumulation, migration and preservation (Masters, 1979; Law and Dickinson, 1985; Reeves et al., 1996; Huang et al., 2017; Nishiyama et al., 2020). Previous studies have presented systematic analyses of the distribution and origin of abnormal pressure. The well-log-based resistivity, soil mechanics principle-based, interval velocity and transit time and equivalent depth methods have been widely used to analyze the vertical distribution of abnormal pressure (Eaton, 1975; Yang et al., 2004; Tingay et al., 2009; Oloruntobi et al., 2018). For the origins of abnormal pressure, disequilibrium compaction, increasing of temperature, mineral transformation, tectonic effects and hydrocarbon generation were stated causes of overpressure (Barker, 1972;

* Corresponding author. State Key Laboratory of Petroleum Resources and Prospecting, China University of Petroleum (Beijing), Beijing, 102249, China.
E-mail address: lindachen@cup.edu.cn (D. Chen).

https://doi.org/10.1016/j.petrol.2021.108601
Received 22 September 2020; Received in revised form 16 February 2021; Accepted 25 February 2021
Available online 9 March 2021

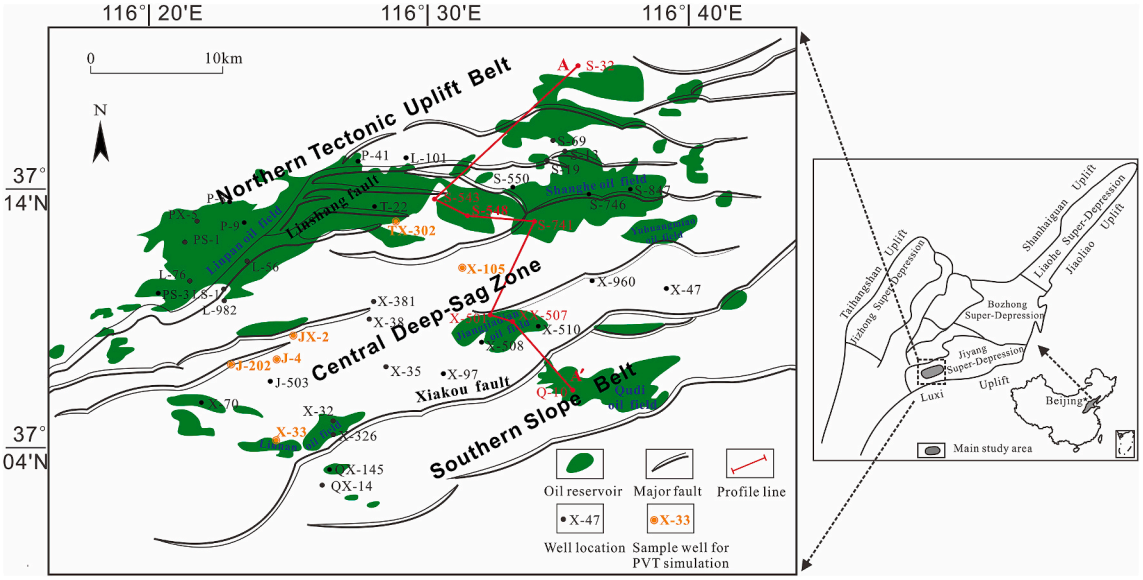

Fig. 1. The location of the Huimin Depression and the main oil field distributions.

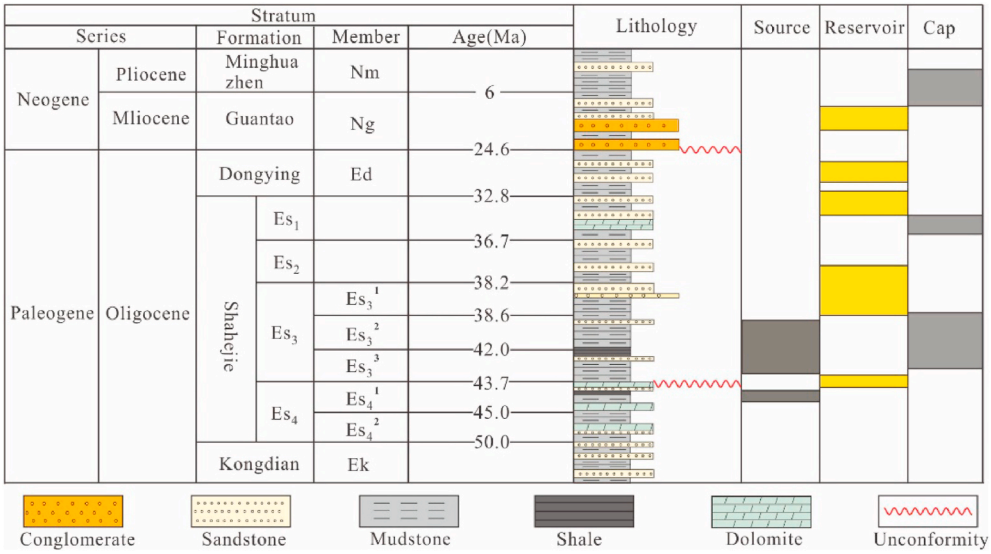

Fig. 2. Generalized stratigraphic column for the Huimin Depression.

Marine and Fritz, 1981; Mouchet and Mitchell, 1989; Moernaut et al., 2017; Liu et al., 2019). Furthermore, rock dilation, thermal effects, groundwater flow, differential gas flow and osmosis were considered the main causes of underpressure (Barker, 1972; Russel, 1972; Neuzil, 2000; Li et al., 2019).

However, in comparison to the distribution and origin, understanding the evolution of abnormal pressure based on paleo-pressure reconstruction is still a challenge in basin analysis because of the limited methods and the great uncertainty in the results. Fluid inclusion analysis has been considered as a major technique for reconstructing paleo-pressure. The homogenization temperature, trapping temperature and salinity of inclusions can be employed to calculate the paleo-pressure (Zhang and Frantz, 1987; Liu et al., 2017), while the trapping temperature in this method cannot be obtained directly. The combination of PVT simulation and equations of state is also effective for the calculation of paleo-pressure (Aplin et al., 1999; Swarbrick et al., 2000; Bourdet et al., 2010; Zhang, 2013). However, this method needs coevally formed petroleum and aqueous inclusions, which has been difficult to satisfy in many situations (Aplin et al., 1999).

The Huimin Depression is characterized by a complex distribution of pore pressure. The pore pressure coefficient, which is defined as the ratio of the tested pore pressure to the hydrostatic pressure at the same depth (abbreviated as Pcoe), ranges from approximately 0.6 to 1.3 in the third member of the Paleogene Shahejie Formation (abbreviated as Es_3) at present (Zhao et al., 2004; Li et al., 2013). According to the classification of abnormal pressure in rift basins in China, overpressure (Pcoe larger than 1.27), normal pressure (Pcoe ranges from 0.96 to 1.06) and underpressure (Pcoe smaller than 0.96) all developed in the E_{S3} in the Huimin Depression (Hao, 2005). Overpressure developed in the central portion of the depression in a depth range from 3500 to 4000 m (Wang et al., 2018), and underpressure developed at the edge of the Huimin depression with a wider depth range from 1300 to 4000 m (Liu, 2011; Liu et al., 2012). Few studies have focused on the evolutionary process of abnormal pressure in the study area, except that by Li et al. (2013), who concluded that the paleo-pressure experienced a periodic rising and falling process from 60 Ma to the present with maximum and minimum pressure coefficients of 1.3 and 0.8, respectively.

The existing studies of the paleo-pressure evolution in the Huimin

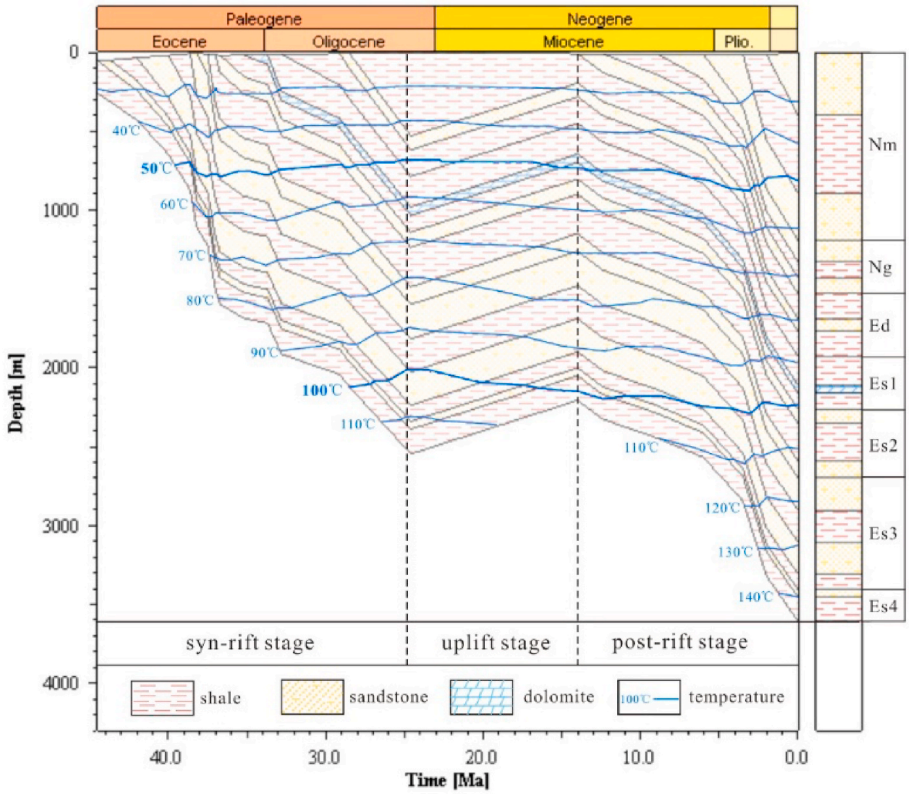

Fig. 3. Burial history in the Huimin Depression.

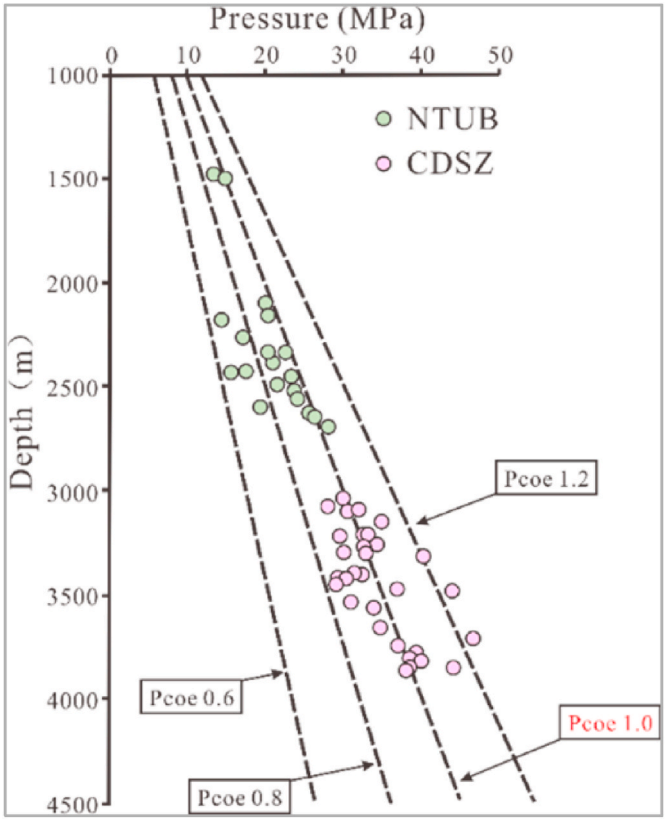

Fig. 4. The distribution of the DSTs data for Es_3 in the Huimin Depression.

Depression have two major problems. One is the reliability of reconstructing paleo-pressure results using a single fluid inclusion method (Li et al., 2013). Another is the lack of correspondence between the evolutionary processes and the origins of abnormal pressure. In this paper, experiments and modeling methods were employed to reconstruct the paleo-pressure of the Es_3 in the Huimin Depression, and the contributions of the major origins of abnormal pressure were analyzed to match the results of the pressure evolution. This study aims to introduce a convincing analysis of the abnormal pressure evolution based on different methods, and the results may be helpful for petroleum exploration in the Huimin Depression.

2. Geological settings

The Huimin Depression is in the southwestern portion of the Jiyang Super Depression, Bohai Bay Basin, in north China. The depression can be divided into Northern Tectonic Uplift Belt (abbreviated as NTUB), Southern Slope Belt (abbreviated as SSB) and Central Deep-Sag Zone (abbreviated as CDSZ) (Fig. 1). It is of the prime oil and gas producing depressions of the Bohai Bay Basin, five commercial oil and gas fields were discovered in the Huimin Depression, which indicated the giant potential of the exploration of the study area.

The sedimentary strata in the Huimin Depression include the Paleogene Kongdian (abbreviated as E_k), the Shahejie (abbreviated as Es), the Dongying Formations (abbreviated as E_d), the Neogene Guantao (abbreviated as N_g) and the Minghuazhen Formations (abbreviated as N_m) (Fig. 2). The Es is subdivided into four members, the fourth (abbreviated as: Es_4), the third (abbreviated as: Es_3), the second (abbreviated as: Es_2) and the first member (abbreviated Es_1) (Fig. 2). The Es is the primary oil and gas producing formation. The source rocks are dark mudstones in semi-deep lacustrine facies in the Es_3 (Li et al., 2014). The total thickness of the source rocks ranges from approximate 150–500 m with the total organic content ranged from 0.5–3% (Zhu and Zeng, 2008; Guo et al., 2009). The main reservoir units are formed by the river-delta sandstone of the Es_3. Additional sandstone reservoirs are

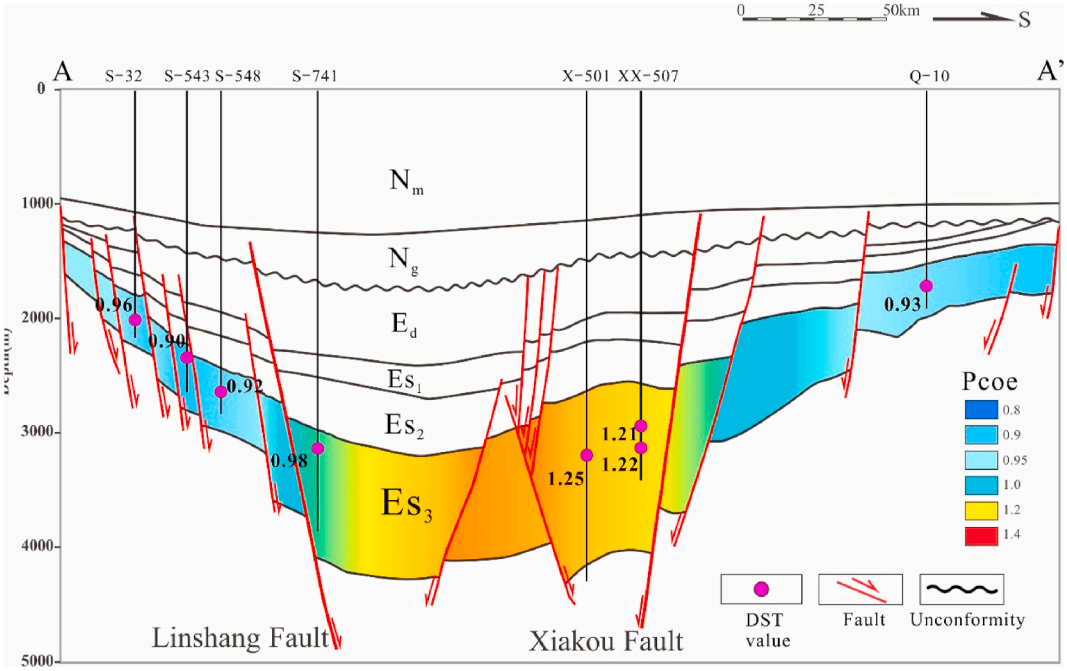

Fig. 5. The vertical Pcoe distribution of Es_3, Huimin Depression (the profile A-A′ is marked in Figs. 1 and 6).

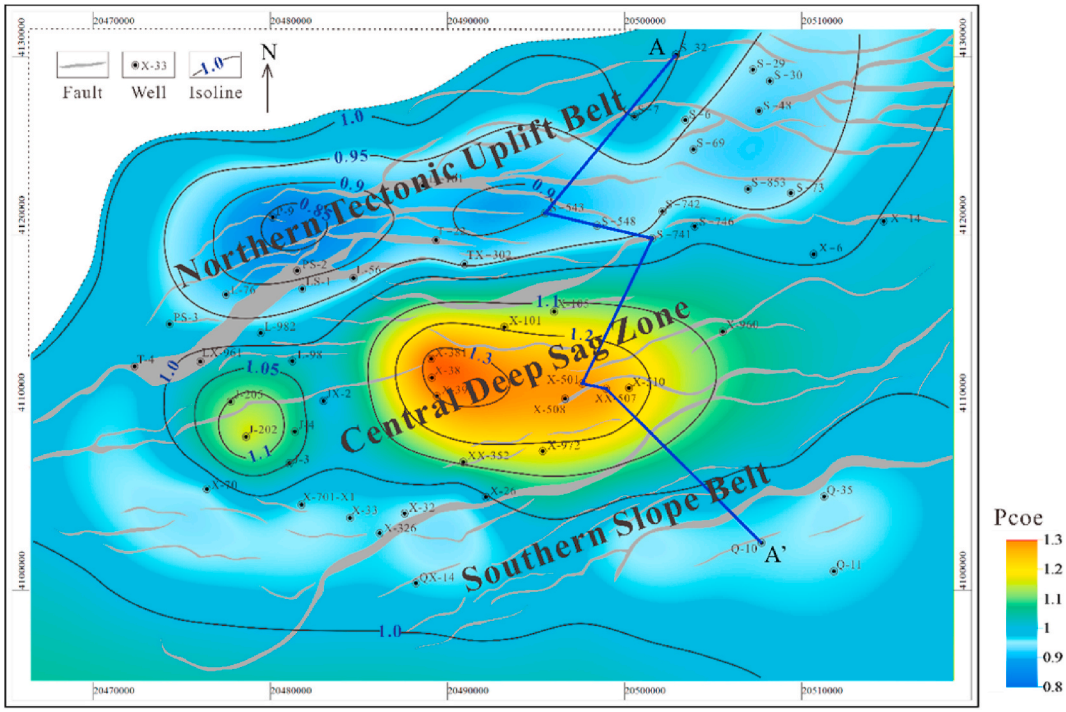

Fig. 6. The contour map of the Pcoe in Es_3, Huimin Depression.

in the Es_2, Es_1, E_d, and N_g (Feng, 2010). The main seal of the reservoirs in the Es_3 is the dark gray mudstone in the Es_2. The main seal of the reservoirs in the Es_2 is the mudstone in the Es_1. The main seal of reservoirs in the Es_1, E_d, and N_g is the mudstone in the N_m.

The tectonic evolution of the Huimin Depression was divided into two stages since the onset of the Cenozoic Era (approximately 65 Ma). The first stage lasted from approximate 60 Ma to 25 Ma, which was a rifting stage characterized by fast deposition of strata with frequent activities of the faults. During the end of the Dongying period (approximate 25Ma to 15 Ma), the tectonic uplift of the entire depression occurred with the erosion of overburden sediments. After uplift and erosion, the Huimin Depression experienced a subsidence phase (Fig. 3). Previous studies indicated that the thermal gradient in the Huimin Depression experienced a decreasing process from approximate 50 to 32 °C/km from the onset of the Shahejie period (approximate 50 Ma) to the present (Qiu et al., 2006).

Table 1
Molar composition of the petroleum inclusions of Well S-32.

Code	C_M[a](%)	Code	C_M[a](%)	Code	C_M[a](%)	Code	C_M[a](%)	Code	C_M[a](%)
N_2	0.675	CO_2	2.241	H_2S	0.046	C_1	32.8	C_2	6.464
C_3	4.201	iC_4	0.765	nC_4	2.27	iC_5	0.797	nC_5	0.95
C_6	0.95	C_7	2.982	C_8	3.562	C_9	2.338	C_{10}	3.766
C_{11}	2.235	C_{12}	0.894	C_{13}	0.447	C_{14}	3.405	C_{15}	0.902
C_{16}	0.897	C_{17}	3.217	C_{18}	0.904	C_{19}	0.626	C_{20}	0.268
C_{21}	1.551	C_{22}	0.894	C_{23}	0.626	C_{24}	0.981	C_{25}	0.894
C_{26}	0.535	C_{27}	1.877	C_{28}	0.049	C_{29}	0.535	C_{30}	0.268
C_{31}	0.089	C_{32}	9.043	C_{33}	0.358	C_{34}	0.224	C_{35}	0.268
C_{36}	0.045	C_{37}	1.34	C_{38}	0.447	C_{39}	0.089	C_{40}	0.01
C_{41}	0.01	C_{42}	0.037	C_{43}	1.225				

[a] C_M: Molar content.

Table 2
Molar composition of the coexisting aqueous inclusions of Well S-32.

Code	C_M[a](%)	Code	C_M[a](%)	Code	C_M[a](%)	Code	C_M[a](%)
N_2	0.002	CO_2	0.030	H_2	0.001	C_1	0.265
C_2	0.006	C_3	0.003	iC_4	0.001	nC_4	0.001
iC_5	0.0001	nC_5	0.0001	H_2O	99.691		

[a] C_M: Molar content.

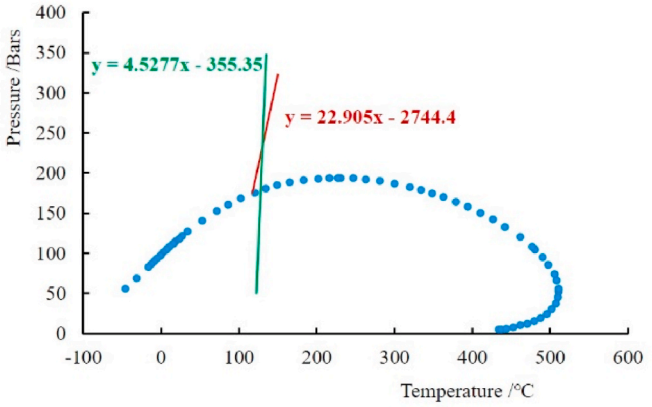

Fig. 7. Phase envelope of petroleum inclusions in Well S-548.

3. Data and methods

3.1. Sampling and data

The abnormal pressure distribution of Es_3 is measured by drill stem tests (DSTs). In this study, a total of 50 pressure data points were provided by Shengli Oilfield Branch of China Petroleum and Chemical Corporation (abbreviated as SOB-CPCC) for analyzing the vertical and lateral distribution of pore pressure in the Huimin Depression.

Samples with fluid inclusions are required for the reconstruction of paleo-pressure. The types, periods, homogenization temperature, volumetric ratio of the liquid and vapor, bulk composition and salinity are important variables that affect the accuracy of the reconstructed paleo-pressure. In this study, 88 core samples from 13 wells covering the NTUB and the CDSZ are used for fluid inclusion analysis. A total of 270 fluid inclusions are identified and analyzed. Among the required data, the types, trapping periods, the homogenization temperature, gas-oil ratio (abbreviated as GOR) and the salinity of fluid inclusions are measured and calculated by the Beijing Research Institute of Uranium Geology (BRIUG) with the LINKAM (THMS600) cooling-heating stage. The molar composition of crude oil and natural gas are obtained using the oil component analysis test data and PVT modeling using simulation software "PVT-Sim" (Mi et al., 2002; Teinturier et al., 2002; Liu et al., 2003).

3.2. PVT simulation method of fluid inclusions

Fluid inclusions record the pore pressure information at which the inclusion is trapped (Roedder, 1984; Goldstein and Raynolds, 1994).

Table 3
Results of the paleo-pressure by the PVT simulation method.

Structural belt	Well	Depth (m)	Th[a] (°C)	F(x)[a]	G(x)[a]	Tt[a] (°C)	Pt[a] (MPa)	Tp (Ma)	Dp (m)	Paleo-Pcoe
NTUB	S-548	3199	118	y = 3.8179x-285.34	y = 9.5801x-1051.7	133	22.24	1.4	2965	0.75
	S-548	3199	110	y = 3.9776x-261.06	y = 18.612x-2090.3	125	23.61	0.8	3027	0.78
	S-548	3270	131	y = 2.0406x-124.12	y = 9.0138x-1211.9	156	19.42	1.2	3184	0.61
	S-548	3270	117	y = 4.5227x-355.35	y = 22.905x-2744.4	130	23.32	18.0	3285	0.71
	S-548	3338	112	y = 1.9727x-24.584	y = 25.701x-2777.1	116	20.43	2.1	3004	0.68
	S-548	3338	110	y = 4.3882x-311.87	y = 37.335x-4430.2	125	23.67	19.2	2959	0.8
	S-548	3381	107	y = 3.8062x-219.14	y = 48.802x-5708.6	122	24.52	0.3	3314	0.74
	S-548	3381	108	y = 6.9967x-613.70	y = 39.380x-4596.8	123	24.69	0.4	3292	0.75
	TX-302	3497	107	y = 6.5014x-493.78	y = 43.373x-4807.8	117	26.69	2.2	3336	0.8
	TX-302	3497	109	y = 9.5764x-871.04	y = 43.695x-4931.3	119	26.86	2.5	3316	0.81
CDSZ	J-202	3793.2	105	y = 13.616x-1262.7	y = 62.248x-7338.5	120	37.12	4.6	3043	1.22
	J-202	3793.2	107	y = 11.435x-1034.0	y = 62.225x-7230.3	122	36.11	3.6	3283	1.1
	J-4	3915	78	y = 11.326x-666.32	y = 67.401x-5881.3	93	38.7	2.6	3518	1.1
	J-4	3915	71	y = 16.526x-999.00	y = 74.443x-5979.9	86	42.25	4.7	3130	1.35
	X-105	3670	118	y = 15.275x-1633.0	y = 69.739x-8876.6	133	39.85	5.2	3266	1.22
	X-33	3286	79	y = 12.928x-857.23	y = 56.431x-4859.4	92	33.21	6.5	2460	1.35
	X-33	3286	97	y = 11.263x-948.63	y = 54.813x-5869.7	113	32.41	5.2	2455	1.32
	JX-2	3816	110	y = 8.929x-806.20	y = 69.849x-9030.3	135	39.92	5.4	2626	1.52
	JX-2	3827	78	y = 10.247x-622.45	y = 52.01x-4422.8	91	31	9.2	2696	1.15

[a] Th is the homogenization temperature, F(x) is the isochore function of the petroleum inclusion, G(x) is the isochore function of the coexisting aqueous inclusion, Tt is the trap temperature, Pt is the trap pressure, Tp is the trapping age of the fluid inclusion, and Dp is the paleo burial depth.

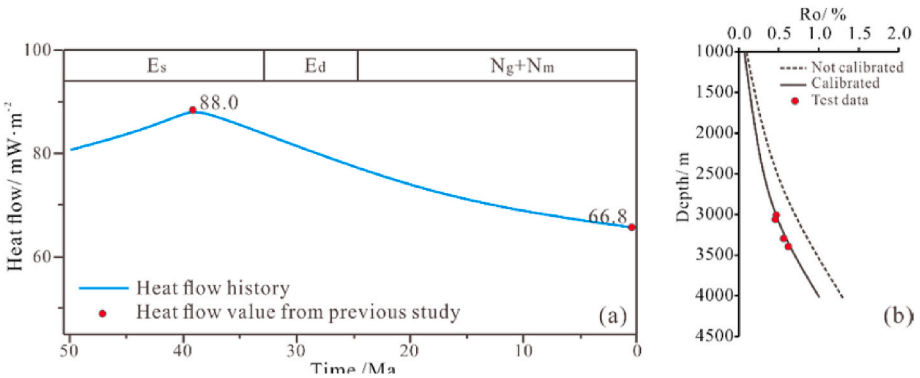

Fig. 8. Determination of the trapping age for Well J-4; (a) heat flow history, where the data of heat flow were from Liu et al. (2019) and (b) heat flow calibration.

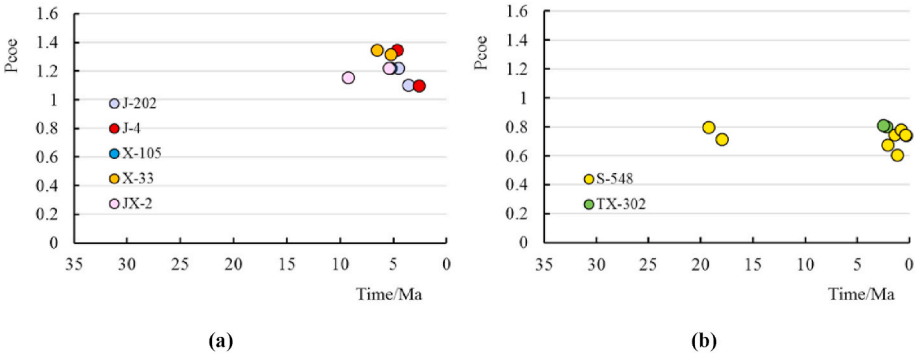

Fig. 9. The paleo-Pcoe values obtained by the PVT simulation method in the (a) CDSZ and (b) NTUB.

However, the trapping pressure (paleo-pressure in this paper) cannot be measured directly. To determine the trapping pressure, P-T phase envelopes and isochores of a petroleum inclusion and its coexisting aqueous inclusion are required (Jawad et al., 2012; McCain, 2017). The construction of the phase envelope requires the molar composition of the inclusions, which can be obtained by the combined use of direct measurement and modeling under PVT conditions with PVT-Sim software (Karlson et al., 1993; Macleod et al., 1994; Aplin et al., 1999). The isochores of inclusions can be modeled and calculated using PVT Sim software and scanning microscopy through a series of processes (Aplin et al., 1999). Therefore, the trapping pressure of the fluids can be obtained by calculating the intersection of a couple of inclusions (the petroleum inclusion and its corresponding aqueous inclusion). In this study, 20 couples of fluid inclusions were analyzed to reconstruct the paleo-pressure.

3.3. Homogenization temperature-salinity method with fluid inclusions

With the limitation of the samples, a continuous evolutionary process for the paleo-pressure cannot be reconstructed using the PVT simulation method. The homogenization temperature-salinity method can be employed for single aqueous inclusions. In this method, the paleo-pressure is considered to have strong links to the trapping temperature and salinity of the geofluids inside the inclusions (Bowers and Helgeson, 1983; Bodnar and Sterner, 1987; Bakker and Doppler, 2016; Liu et al., 2018a, 2018b). The constant volume formula, which contains the data for the homogenization temperature, trapping temperature, and salinity of fluids, is proposed to calculate the paleo-pressure (Zhang and Frantz, 1987; Driesner and Heinrich, 2007; Bakker, 2018):

$$P = A_1 + A_2 \times T \tag{1}$$

where P is the trapping pressure, 10^{-1} MPa, and T is the trapping temperature, which will be discussed in detail in Section 5.1.2. A_1 and A_2 are parameters that can be calculated as follows:

$$A_1 = 6.1 \times 10^{-3} + \left(2.385 \times 10^{-1} - a_1\right) \times T_h - \left(2.855 \times 10^{-3} + a_2\right) \times T_h^2 - \left(a_3 \times T + a_4 \times T_h^2\right) \times \mathrm{m} \tag{2}$$

$$A_2 = a_1 + a_2 \times T_h + 9.888 \times 10^{-6} \times T_h^2 + (a_3 + a_4 \times T_h) \times m \tag{3}$$

where a_1 = 28.48, a_2 = -6.445 × 10^{-2}, a_3 = -0.4159 and a_4 = 7.438 × 10^{-3} are the parameters determined by the ground water system (Zhang and Frantz, 1987), which is a NaCl-H_2O-type in the Huimin Depression (Liu et al., 2013); T_h is the homogenization temperature measured by BRIUG; and m is the molar concentration of salts in the fluid of the inclusion. The conversion of m from the salinity of fluid inclusions can be presented in Eq. (4) as

$$\mathrm{m} = \frac{1000 \times \omega}{58.5 \times (100 - \omega)} \tag{4}$$

where ω is the salinity of inclusions measured by BRIUG.

This method could provide more paleo-pressure data comparing with the PVT simulation method. In this study, 256 inclusions were analyzed to obtain the paleo-pressure via this method.

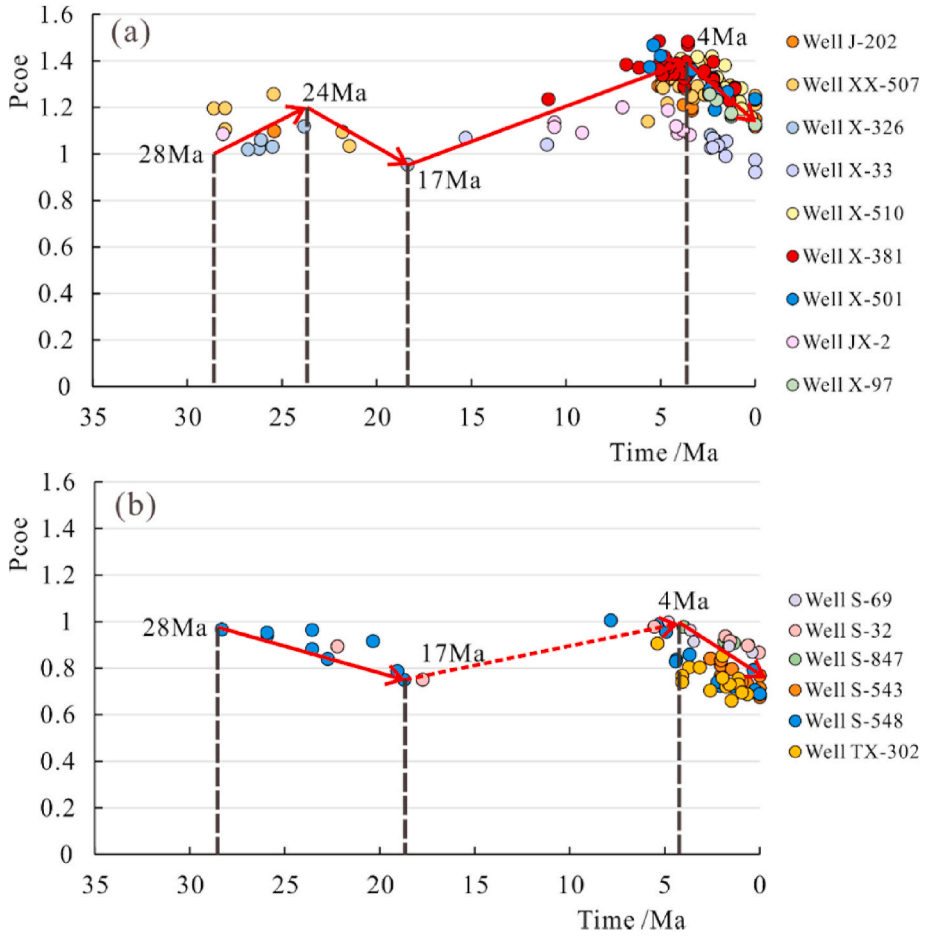

Fig. 10. Evolution of Pcoe from the homogenization temperature-salinity method in the (a) CDSZ and (b) NTUB.

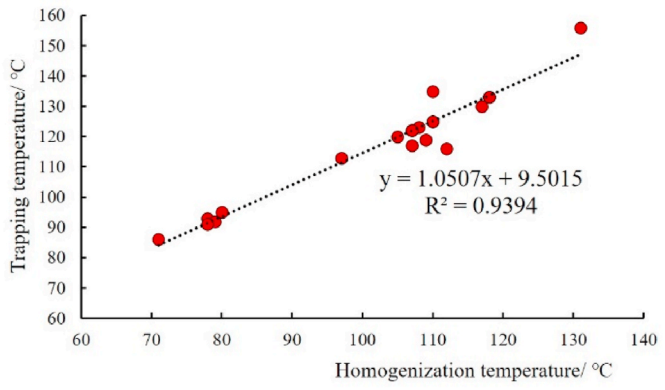

Fig. 11. The relation between the trapping temperature and the homogenization temperature obtained by PVT Sim methods.

3.4. Basin modeling method

Basin modeling software is employed to provide models for geological processes based on a series of geological background data (sedimentary and erosion events, thickness of the strata, detailed lithology, etc.), foundational equations, boundary conditions and relating analyses (Gac et al., 2018; Hakimi et al., 2018; Abdelwahhab and Reaf, 2020; Carvajal-Arenas et al., 2020). Based on tectonic and sedimentary process analyses, 1D model by basin modeling can provide the pressure-depth distribution (Abdel-Fattah et al., 2017; Al-Khafaji et al., 2021). The abnormal pressure calculated by the porosity reduction model in a 2D model can reflect the overpressure generated by mechanical compaction with consideration of lateral transfer (Swarbrick et al., 2000). The calibration of thermal history and physical properties can improve the accuracy of the modeling results (Qiu et al., 2016; Hakimi et al., 2019). In this study, basin modeling simulators PetroMod 2D were employed for overpressure evolution by the effect of compaction.

4. Results

4.1. The abnormal pressure distribution in the Es_3

The DSTs data indicate that the overpressure, normal pressure and underpressure all developed in the Huimin Depression. The NTUB is characterized by underpressure to normal pressure with a depth that ranges from approximately 2000 to 2700 m and Pcoe from 0.6 to 1.0. In contrast, the CDSZ is characterized by underpressure, normal pressure and overpressure with a depth that ranges from approximately 3000 to 4000 m and Pcoe from 0.8 to 1.2 (Fig. 4).

The overpressure mainly distributes in the CDSZ with a limited range centered on Well X-381 and Well X-501 (Figs. 5 and 6). The Pcoe of the overpressure area ranges from 1.2 to 1.3. The NTUB is characterized by a wider underpressure range covering almost all of the belt with Pcoe from approximately 0.85 to 0.9, while the SSB is characterized by a limited underpressure area with Pcoe from 0.9 to 0.95. The boundary faults, including northern Linshang Fault and southern Xiakou Fault show lateral sealing capacity, which can be barriers for fluid flow and hence preserving the overpressure in the CDSZ (Li and Liu, 2013; Wang et al., 2019).

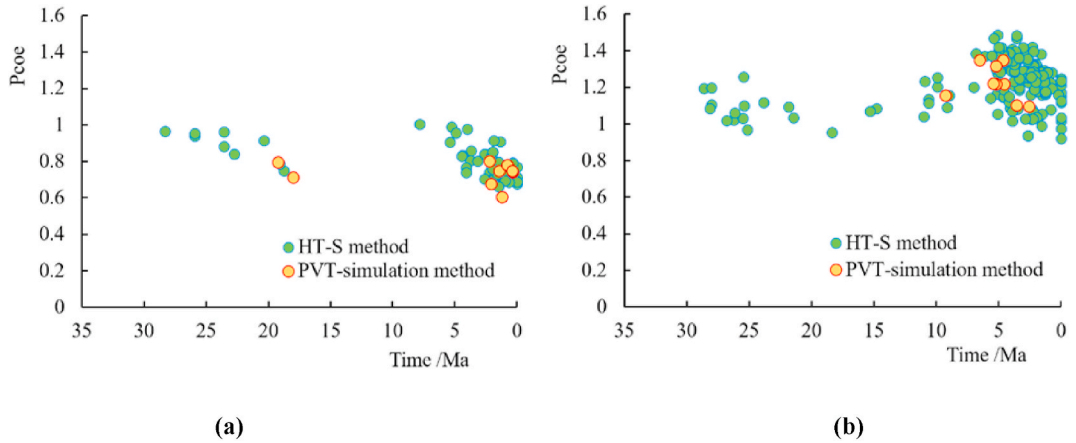

Fig. 12. The relationship between the paleo-Pcoe obtained by the PVT simulation method and the homogenization temperature in the (a) NTUB and (b) CDSZ.

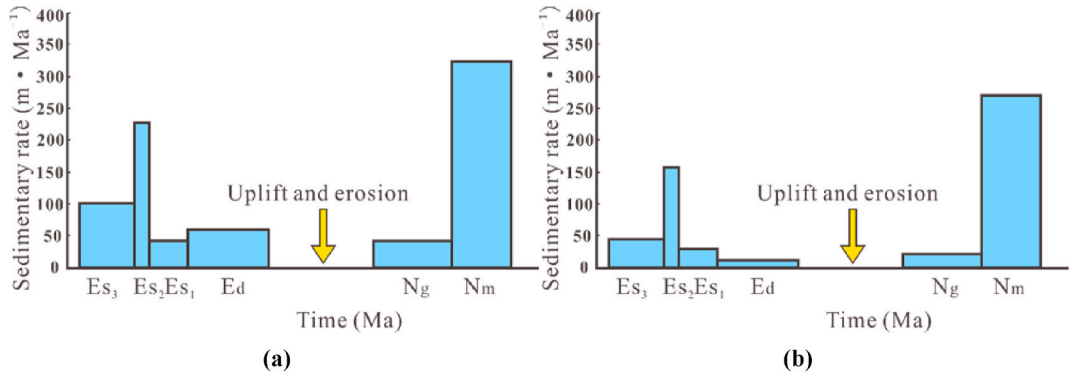

Fig. 13. Sedimentary rate of formations in (a) Well XX-507 and (b) Well S-32, the location of wells is showed in Fig. 1.

4.2. The paleo-pressure from PVT simulations

In this paper, a total of 19 pairs of fluid inclusions were observed and employed to obtain the trapping temperature and paleo-pressure. Among these samples, 10 are from the NTUB, and the other 9 are from the CDSZ (Fig. 1). The molar composition of C_1 to C_7 in the petroleum inclusions was derived from the testing data of the petroleum composition of the oil in the Huimin Depression, and C_8 to C_{40} were simulated by PVT Sim software. The molar compositions of the corresponding aqueous inclusions were directly provided by using oilfield testing data of the molar composition of natural gas. (Tables 1 and 2).

With the molar composition of fluid inclusions, phase envelopes and isochores of petroleum inclusions and their coexisting aqueous inclusions can be reconstructed (Fig. 7). By calculating the intersection of the couples of isochores, the trapping pressure and trapping temperature were obtained (Table 3). The determination of the trapping age of the fluid inclusion requires the formation temperature data, which can be affected by the heat flow history. In this research, the heat flow history was set using previous studies for thermal history research in the Bohai Bay Basin (Ding et al., 2008; Peng and Zou, 2013; Liu and He, 2019). The temperature history obtained from heat flow history was calibrated using vitrinite reflectance (Ro) data (Fig. 8). Considering the lack of data for heat flow, present-day data for some individual wells were obtained from the adjacent well or the average heat flow value of the whole tectonic zone. Combined with the burial history of individual wells, the trapping age of the inclusions was derived, and the evolution of the paleo-pressure was reconstructed (Fig. 9). From the results, the inclusions in the NTUB are characterized by underpressure with the Pcoe ranging from approximately 0.6 to 0.8, and showing a tendency to decrease from 20 to 17 Ma and 3 to 0 Ma. However, inclusions in the CDSZ are dominated by overpressure to normal pressure with Pcoe ranging from approximately 1.0 to 1.4 and characterized by a tendency to decrease from 5 to 0 Ma.

4.3. The paleo-pressure from the homogenization temperature-salinity calculation

With the limitation of the samples, a continuous evolutionary process of the paleo-pressure cannot be reconstructed by the PVT simulation method. The homogenization temperature-salinity method can be employed for single aqueous inclusions. In this study, 256 aqueous inclusions were used to provide a continuous evolutionary process of paleo-pressure.

The results show different evolutionary processes of the paleo-pressure in different structure belts. The paleo-pressure in the CDSZ was characterized by two rising and two falling stages from approximately 28 Ma to the present (Fig. 10a). Paleo-Pcoe in the first rising stage from 28 Ma to 24 Ma rose from approximately 1.0 to 1.2, followed by a falling stage from 24 Ma to 17 Ma, which caused it to fall to approximately 1.0. During the second rising stage from 17 Ma to 4 Ma, the paleo-Pcoe rose to 1.2 to 1.5 and finally fell to 1.0 to 1.3 from 4 Ma to the present. However, the paleo-pressure in the NTUB was characterized by two falling stages (Fig. 10b). The paleo-Pcoe first fell from approximately 1.0 to 0.7 during 28 Ma to 17 Ma. Then, during the second falling stage, it fell from approximately 4 Ma to the present from 1.0 to approximately 0.6–0.9.

Table 4
Lithologies of the formations in the Huimin Depression.

Strata/ event	Begin age (Ma)	Lithology	
		Well-XX-507	Well-S-32
Nm_1	4.1	Sandstone (typical)-100%	Sandstone (typical)-100%
Nm_2	6	Shale (typical)-100%	Shale (typical)-100%
Ng_1	8.6	Sandstone (typical)-100%	Sandstone (typical)-100%
Ng_2	10.9	Shale (typical)-100%	Shale (typical)-100%
Ng_3	14	Sandstone (typical)-100%	Sandstone (typical)-100%
Erosion	24.6	/	/
Ed_1	27.9	Shale (organic lean, sandy)-50%, Sandstone (subarkose, quartz rich)-50%	Sandstone (arkose, typical)-100%
Ed_2	32.8	Sandstone (subarkose, quartz rich)-100%	
Es_1^1	34	Shale (organic lean, sandy)-70%, Sandstone (arkose, quartz rich, 30%)	Shale (typical)-50%, Sandstone (arkose, typical)-50%
Es_1^2	35.1	Dolomite (organic lean, silty)-100%	Dolomite (organic lean, silty)-100%
Es_1^3	36.7	Shale (organic lean, sandy)-70%, Siltstone (organic lean)-30%	Shale (typical)-50%, Siltstone (organic lean)-50%
Es_2^1	37.6	Sandstone (arkose, typical)-100%	Sandstone (arkose, typical)-100%
Es_2^2	38.2	Shale (organic lean, typical)-100%	Shale (organic lean, typical)-100%
Es_3^1	38.6	Sandstone (arkose, typical)-30%, Siltstone (organic lean)-70%	Sandstone (arkose, typical)-100%
Es_3^2	42	Siltstone (organic rich, typical)-50%, Shale (organic rich, typical)-50%	Shale (typical)-50%, Siltstone (organic lean)-50%
Es_3^3	43.7	Shale (organic rich, 3% TOC)-70%, Shale (typical)-30%	Shale (organic lean, typical)-100%
Es_4	45	Shale (typical)-100%	Shale (typical)-100%

Table 5
The excess pressure evolution of Well XX-507 by disequilibrium compaction in the CDSZ.

Time (Ma)	32.8	24.6	14	6	0
Excess pressure (MPa)	0.06	3.99	2.03	3.79	8.88

5. Discussion

5.1. Error analysis and accuracy evaluation

In this paper, two methods were employed for the analysis of the abnormal pressure evolution. Considering the limitations of the mechanism of each method and the inconsistencies between the calculated results and measured data, an error analysis and accuracy evaluation are required.

5.1.1. PVT simulation method

The pressure value error of the PVT simulation method is mainly derived from the determination of bulk compositions and the ratio of the liquid to the vapor of the inclusions (Aplin et al., 1999). As shown previously, the bulk composition was determined by PVT Sim software and detailed testing data for the molar composition of oil and gas were from SOB-CPCC, and the ratio of the liquid to the vapor data was measured by BRIUG. The good match between the present pressure results provided by this method and the pressure data from the DSTs demonstrates the accuracy and reliability of this method for paleo-pressure evaluation (Figs. 4 and 9).

However, the determination of the trapping age may lead to some errors in the paleo-pressure evolution. The paleo-pressure evolution based on fluid inclusions only provides a dispersed distribution of pressure values (Mi et al., 2002; Liu et al., 2012). This dispersed distribution may lead to some deviation to the determination of the turning point of the pressure evolution. Hence, the paleo-pressure evolutionary process by fluid inclusion methods needs to be adjusted based on geological processes.

5.1.2. Homogenization temperature-salinity method

From Eq. (1)-Eq. (4), the pressure value of the homogenization temperature-salinity method is related to the values of the homogenization temperature, trapping temperature and salinity of the fluid inclusions. In this study, the trapping temperature is of great importance for the accuracy of this method. Some studies have stated that the trapping temperature had a linear relationship with the homogenization temperature (Mi et al., 2002; Liu et al., 2016a, 2016b, 2016c). A previous analysis in this paper shows that the trapping temperature can be determined by the calculation of the intersection of the petroleum inclusion and its coexisting aqueous inclusions by using the PVT simulation method. The result indicates that there is a good positive relationship between the homogenization temperature and the trapping temperature (Fig. 11). Thus, the trapping temperature of inclusions in the homogenization temperature-salinity method can be determined. The good match of the paleo-pressure calculation between the PVT simulation method and homogenization temperature-salinity method (Fig. 12) and of the present pressure between the homogenization temperature-salinity method and the pressure data for the DSTs show that the paleo-pressure value calculated by this method is acceptable (Figs. 4 and 10). However, the determination of the trapping age using this method may also lead to some errors in the pressure evolution, as analyzed in the former section. The pressure evolution obtained by this method also needs to be adjusted by the geological processes in the Huimin Depression.

5.2. Relationships between the origins and evolution of abnormal pressure

The results of paleo-pressure reconstruction by using fluid inclusions methods show similar evolutionary processes. However, the rationality of paleo-pressure evolution needs to be checked and analyzed by the analysis of abnormal pressure origins and the quantitative evaluation for the contribution of each origin to the abnormal pressure.

5.2.1. Origins of overpressure

5.2.1.1. Disequilibrium compaction. Disequilibrium compaction is considered as a common origin of overpressure (Burrus, 1998; Law and Spencer, 1998; Swarbrick and Osborne, 1998). Under conditions of the rapid burial of sediments, the fluids in the low-permeability rocks cannot be expelled in time, leading to increases in pore pressures (Magara, 1975; Mouchet and Mitchell, 1989; Tingay et al., 2009). As shown in Fig. 13, the sedimentation rate in the CDSZ can reach approximate 220 m/Ma during the Shahejie period (Fig. 13a). In contrast, the sedimentation rate in the NTUB was approximate 150 m/Ma during the Shahejie period (Fig. 13b). Previous studies showed that only if the sedimentation rate of the strata is larger than approximate 200 m/Ma could disequilibrium compaction develop resulting in overpressure (Burrus, 1998; Heppard et al., 1998; Zhang, 2019). Therefore, the overpressure of disequilibrium compaction mainly developed in the CDSZ.

In this study, a 2D model obtained by the basin modeling method for profile A-A' (shown in Fig. 5) was employed to analyze the evolution of the overpressure by disequilibrium compaction. The lithologies of the strata in the Huimin Depression show differences between the CDSZ and the NTUB. For the accuracy of the lithologies, the strata were divided into several members or submembers. From the bottom to the top, the Es_3 was divided into 3 submembers (abbreviated as Es_3^3, Es_3^2 and Es_3^1);

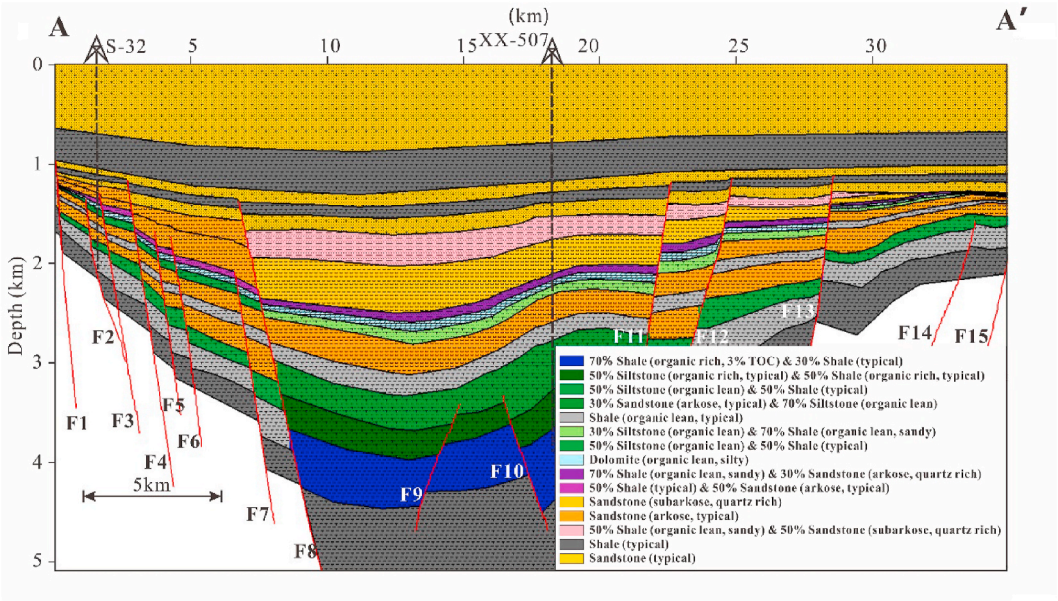

Fig. 14. Lithologies of profile A-A′ for 2D modeling by PetroMod Software.

The Es_2 was divided into 2 submembers (abbreviated as Es_2^2 and Es_2^1); The Es_1 was divided into 3 submembers (abbreviated as Es_1^3, Es_1^2 and Es_1^1); The Ed was divided into 2 members (abbreviated as Ed^2 and Ed^1); The Ng was divided into 3 members (abbreviated as Ng_3, Ng_2 and Ng_1). The N_m was divided into 2 members (abbreviated as Nm_2 and Nm_1). The lithologies for profile A-A' were set by mixed lithologies according to published articles (Sun et al., 2008; Li et al., 2014, 2018), as well as log data and reservoir report data provided by SOB-CPCC. (Table 4 and Fig. 14). The required boundary conditions of the basal heat flow and paleo water depth were obtained from published research (Xie et al., 2009; Liu et al., 2012; Peng et al., 2013). The sediment water face temperature (SWIT) was obtained using PetroMod software for the study area (Eastern Asia, latitude 37°) (Wygrala, 1989). Furthermore, the characteristics of faults were decided by the shale gouge ratio (Yielding et al., 1997).

The calibration of the pore pressure focused on the key submembers of Es_2^2 and Es_3 (Es_3^1, Es_3^2, Es_3^3) in the CDSZ, which were characterized by abnormal pressure Hantschel et al., 2009). First, the depth-porosity profile of each key layer in the Es_3 was generated using a compressibility model, which characterized the porosity-depth relationship based on the compaction law(Hantschel et al., 2009). Then, the porosity-depth relationship was fitted by measured porosities in the NTUB and the CDSZ (Fig. 15a, b, c, and d). Second, the modeling pore pressure was calibrated by adjusting the porosity-permeability relationship generated by the multipoint permeability model, which was provided by the software, and the porosity-permeability relationship was characterized by testing porosity-permeability data pairs (Fig. 16a, b, c, and d).

The 2D model of the overpressure evolutionary process showed large differences between the CDSZ and the NTUB (Fig. 17).

(1) From 36.7 to 32.8 Ma, overpressure mainly developed in the low-permeable rocks the Es_3^3 in the CDSZ, and the NTUB was characterized by normal pressure (Fig. 17a and b).
(2) From 32.8 Ma to 24.6 Ma, the overpressure of the Es_3^3 in the CDSZ increased to approximately 25 MPa, and the overpressure in the Es_3^2 also developed. With the low-permeable pressure seal of the Es_2^2, a weak overpressure of approximately 2 MPa was maintained in the Es_3^1. The NTUB was still characterized by normal pressure (Fig. 17c).
(3) From 24.6 to 14 Ma, the whole depression experienced uplift and erosion. The overpressure slightly decreased in all depressions (Fig. 17d).
(4) From 14 to 6 Ma, the overpressure of the Es_3^1, Es_3^2 and Es_3^3 in the CDSZ gradually increased again at a relatively slow speed. The overpressure in the Es_3^1 reached approximately 2–3 MPa at 6 Ma. The NTUB was also dominated by normal pressure (Fig. 17e).
(5) From 6 Ma to the present, the overpressure of the Es_3^1 and Es_3^2 in the CDSZ increased rapidly. Owing to the low-permeable pressure seal of the Es_2^2, an overpressure of approximately 8 MPa was maintained in the Es_3^1. In the NTUB, overpressure developed in the Es_3^3 in some deep burial regions, while the Es_3^2 and Es_3^1 were both characterized by normal pressure (Fig. 17f). The model showed that disequilibrium compaction led to overpressure of 8.88 MPa in the CDSZ of the Huimin Depression (Table 5).

5.2.1.2. Hydrocarbon generation. Hydrocarbon generation is considered to be a substantial origin of overpressure (Durand, 1983; Lash and Englender, 2005; Guo et al., 2011a, 2011b; Peng et al., 2013). The generation of hydrocarbons in source rocks leads to overpressure because the volume of the generated hydrocarbons is greater than the volume of the original solid kerogen (Hedberg, 1974; Meissner, 1978; Law and Bostick, 1980). When the overpressure in the source rocks is sufficiently large, microfractures develop in the source rocks, and overpressured fluids with hydrocarbons are injected into contacted high-permeable reservoir rocks with a high rate flow, which will lead to an increase in the pressure in a short time (Roberts and Nunn, 1995; Caillet et al., 1997; Peng et al., 2013). The dominate source rock in the Huimin Depression is the deeply buried shale of the Es_3, which is located in the CDSZ. Hence, overpressure by hydrocarbon generation should only develop in the CDSZ of the Huimin Depression from the source rocks to the above reservoirs because of the buoyancy.

Previous studies have provided several calculation models for excess pressure caused by hydrocarbon generating process (Meissner, 1978; Bredehoeft et al., 1994; Guo et al., 2010, 2011a, 2011b). In this study, the quantitative method introduced by Guo et al. (2011a, 2011b) was selected considering the accuracy and the data required by different methods. The excess pressure by hydrocarbon generation is expressed by Eqs. (5) and (6) as follows:

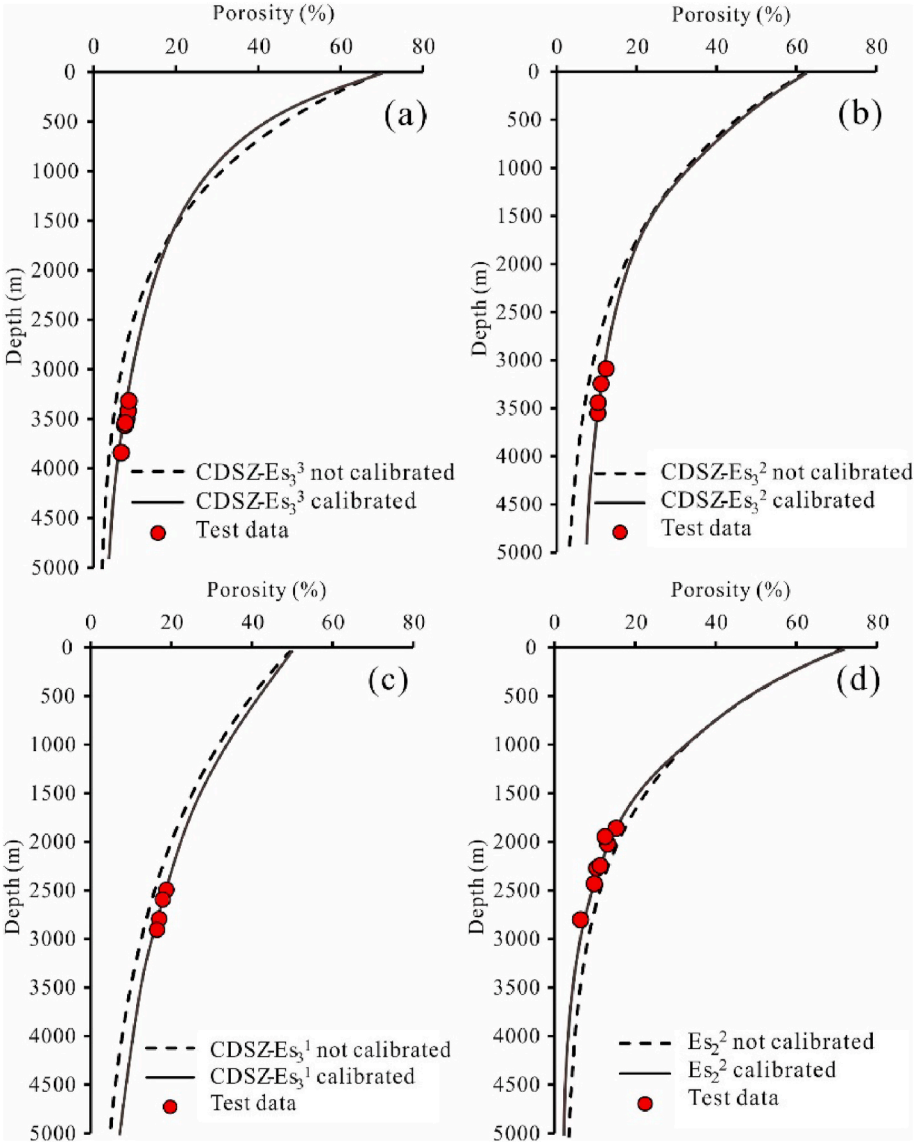

Fig. 15. Calibration of the porosity in the 2D model.

$$P = \frac{IF\mathrm{M}_k[\alpha \mathrm{D}(1 - P_h \mathrm{C}_o) - 1]}{\mathrm{C}_w \mathrm{V}_{w1}\rho_k + (1 - IF)\mathrm{C}_k \mathrm{M}_k + aIF\mathrm{M}_k \mathrm{DC}_o} \quad (5)$$

$$\mathrm{D} = \rho_k / \rho_o \quad (6)$$

where P is the excess pressure, MPa; I is the hydrogen index, mg/g; F is the transformation ratio of the source rocks, dimensionless; M_k is the kerogen mass, kg; α is the residual oil coefficient, dimensionless; P_h is the hydrostatic pressure of a certain depth, MPa; C_o is the oil compressibility, MPa^{-1}; C_w is the water compressibility, MPa^{-1}; V_{w1} is the pore water volume without oil generation, ml; ρ_k is the density of kerogen, $\mathrm{kg/m}^3$; C_k is the kerogen compressibility, MPa^{-1}; and ρ_o is the density of the crude oil, $\mathrm{kg/m}^3$.

In Eq. (1), F is determined by the vitrinite reflectance (abbreviated as Ro) of the source rocks and the type of kerogen by using the kinetic model in the PetroMod software (Burnham et al., 1987). α is obtained by the kinetics of petroleum generation with GOR-Evaluation software (Sweeney and Burnham, 1990; Tang and Stauffer, 1994). In this study, α is 0.85 and is obtained from the available literature (Guo et al., 2009). The value of C_o is 2.2×10^{-3} MPa^{-1} (McCain, 2017), and C_w is 0.44×10^{-3} MPa^{-1} (Amyx et al., 1960). V_{w1} is determined by the porosity of the source rock, which is calculated using PetroMod software by the Reciprocal Compaction Model (Falvey and Middleton, 1981). ρ_k is 1200 $\mathrm{kg/cm}^3$, and C_k is 1.4×10^{-3} MPa^{-1} (Dubow, 1984). ρ_o is 900 $\mathrm{kg/cm}^3$ (McCain, 2017). Ro is also a required parameter, and a relationship between the burial depth and tested Ro is established (Fig. 18). The testing data for Ro are provided by SOB-CPCC. The measured Ro showed a relative strong positive relation to the burial depth of the source rock with the R^2 of approximate 0.8. Therefore, the value of paleo-Ro can be calculated by burial depth.

The source rock of the Huimin Depression is the dark mudstone in the CDSZ. Previous studies showed that the hydrocarbon generation started at the depth of 2400m and reached the peak at the depth of approximate 3500m (Zhu and Zeng, 2008). From the burial history, hydrocarbon generation in the CDSZ started at approximate 10Ma and had the maximum intensity from 10 to 3 Ma. Since 3 Ma, the intensity of hydrocarbon generation gradually weakened and stopped (Fig. 19) (Guo et al., 2009).

In this study, Well XX-507 in the CDSZ and Well S-32 in the NTUB were selected to calculate the excess pressure from hydrocarbon generation in the Es_3^3 source rocks. The results show that overpressure from oil generation only exists in Well-XX-507 in the CDSZ. Overpressures for a unit mass have gradually increased and reached 6.39 MPa for Well XX-507 from approximate 6Ma to the present. While, there is no

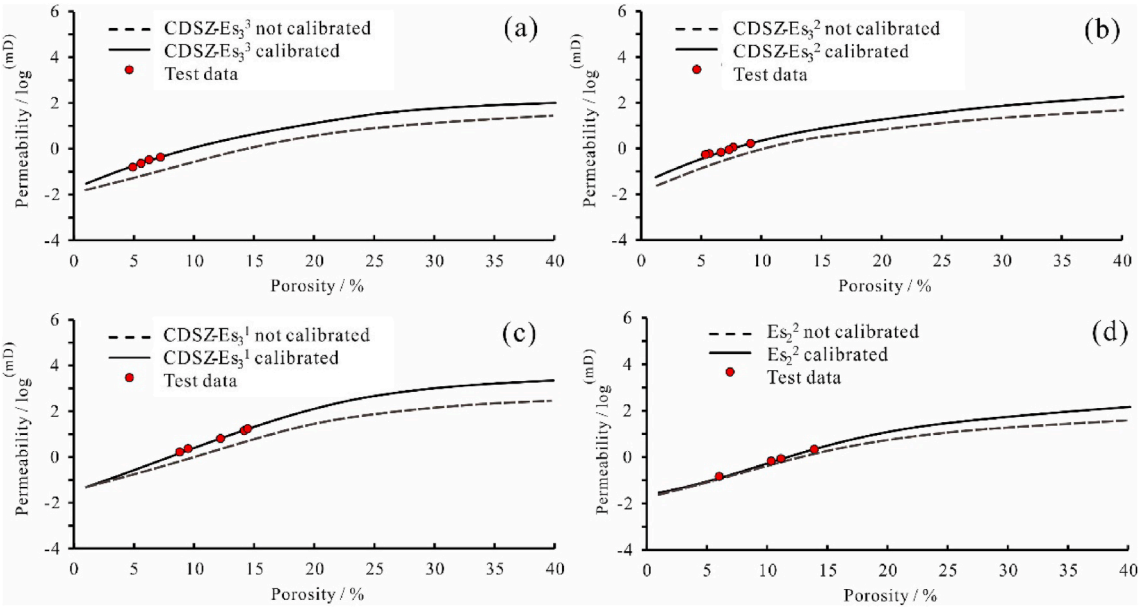

Fig. 16. Calibration of the permeability in the 2D model.

overpressure developed from hydrocarbon generation in Well S-32 in the NTUB because the Ro has not reached the mature window (Table 6).

5.2.2. Origins of underpressure

5.2.2.1. Elastic rebound of rocks. The erosion of strata causes the overburden stress to decrease, which can lead to the elastic rebounding process of the rock matrix and hence increasing the porosity. The increase in pore volume, which is not taken into account by the porosity reduction model used in the PetroMod software, produces underpressure (Russel, 1972; Corbet and Bethke, 1992; Luo and Vasseur, 1995; Stefan and Underschultz, 1995). The Huimin Depression had experienced a period of unbalanced uplift and stratum erosion from approximate 25 Ma to 15 Ma, which caused the elastic rebound of rocks and associated underpressure. Previous studies have provided a quantitative evaluation for the underpressure due to the elastic rebound at the end of erosion (Li et al., 2013; Liu et al., 2018a, 2018b; Wang et al., 2019):

$$\Delta P_{ER} = -\frac{1}{3}\frac{1+v}{1-v}\frac{C_r}{C_r + C_w}\rho_r g \Delta Z \tag{7}$$

where ΔP_{ER} is the decreased pressure due to the elastic rebound of rocks, Pa;v is the Poisson's ratio of the rocks, dimensionless; C_r is the compressibility of sandstone, MPa^{-1}; C_w is the compressibility of water, MPa^{-1}; ρ_r is the rock density (g/cm^3); g is the acceleration of gravity, m/s^2; and ΔZ is thickness of erosion, m.

In this study, the value of v is 0.2 (Xie et al., 2003), C_r is 1×10^{-3} MPa^{-1} (Fatt, 1958; Russel, 1972), and C_w is 3×10^{-4} MPa^{-1} (Russel, 1972). ΔZ and ρ_r are provided by SOB-CPCC. From Eq. (3), ΔZ is the decisive factor for ΔP_{ER}. The NTUB is characterized by intense erosion, with most of ΔZ ranging from approximately 500 to 800 m (Su et al., 2006), while ΔZ in the CDSZ is almost less than 200 m (data from SOB-CPCC) (Table 7).

The results indicate that the elastic rebound of rocks caused underpressure of approximately 6.50 MPa in the NTUB and 1.71 MPa in the CDSZ from 24.6 to 14 Ma. The calculation results indicate that the effect of the elastic rebound of rocks is the dominant reason for underpressure of the NTUB.

5.2.2.2. Temperature reduction. The formation temperature influences pore pressure by controlling the volume of pore fluids (Hodgman, 1957). The reduction of temperature leads to a volumetric contraction of the rock framework and pore fluids. The more intense contraction of pore fluid (dominated by water formation) than the rock framework results in the underpressure in stratum (Law and Spencer, 1998; Xie et al., 2003; Wang et al., 2019).

The tectonic process of uplift and stratum erosion can cause the temperature reduction by shallowing the burial depth in the study area from approximately 24.6 to 14 Ma (Fig. 2). The burial history indicated that the underpressure caused by the shallow burial depth in the Huimin Depression was offset and finally disappeared by the temperature rising from the subsequent deposition of strata. The difference in volume contraction between the pore fluids and rock framework can be expressed as follows (Li et al., 2013; Liu et al., 2018a, 2018b):

$$\Delta V = \Delta T[a_w \phi + a_r(1-\phi)] \tag{8}$$

where ΔV is the volume reduction, m^3; ΔT is the decreasing of formation temperature, K; a_w is defined as the thermal expansion coefficient of the formation water, 4×10^{-8} K^{-1} (Hodgman, 1957); a_r is defined as the thermal expansion coefficient of rocks, 9×10^{-6} K^{-1} (Hodgman, 1957); and ϕ is the porosity of the porous rock, dimensionless.

The reduction of pressure by temperature reduction is given by Pascal's Law:

$$V = V_0(1 - C_w \Delta P_{TR}) \tag{9}$$

where V represents the pore fluid volume after temperature reduction, m^3; V_0 represents the initial pore fluid volume, m^3; and ΔP_{TR} is the reduction of pressure by temperature reduction, MPa. In petroleum geology, the porosity of the rocks is considered as the initial pore fluid volume of the rocks, Equation (10) can be transformed as follows.

$$\Delta P_{TR} = \frac{\Delta V}{C_w \times \phi} \tag{10}$$

In this study, ΔT is determined by the difference between the formation temperature before and after the tectonic uplift of strata. The evolution of the thermal gradient and burial history with an estimate of erosion thickness being required, as shown in Fig. 20 and Table 8. The result reveals a more intense underpressure in the NTUB with an average of 2.11 MPa than that in the CDSZ with an average of 0.55 MPa. In the NTUB and the CDSZ, underpressure by temperature reduction existed

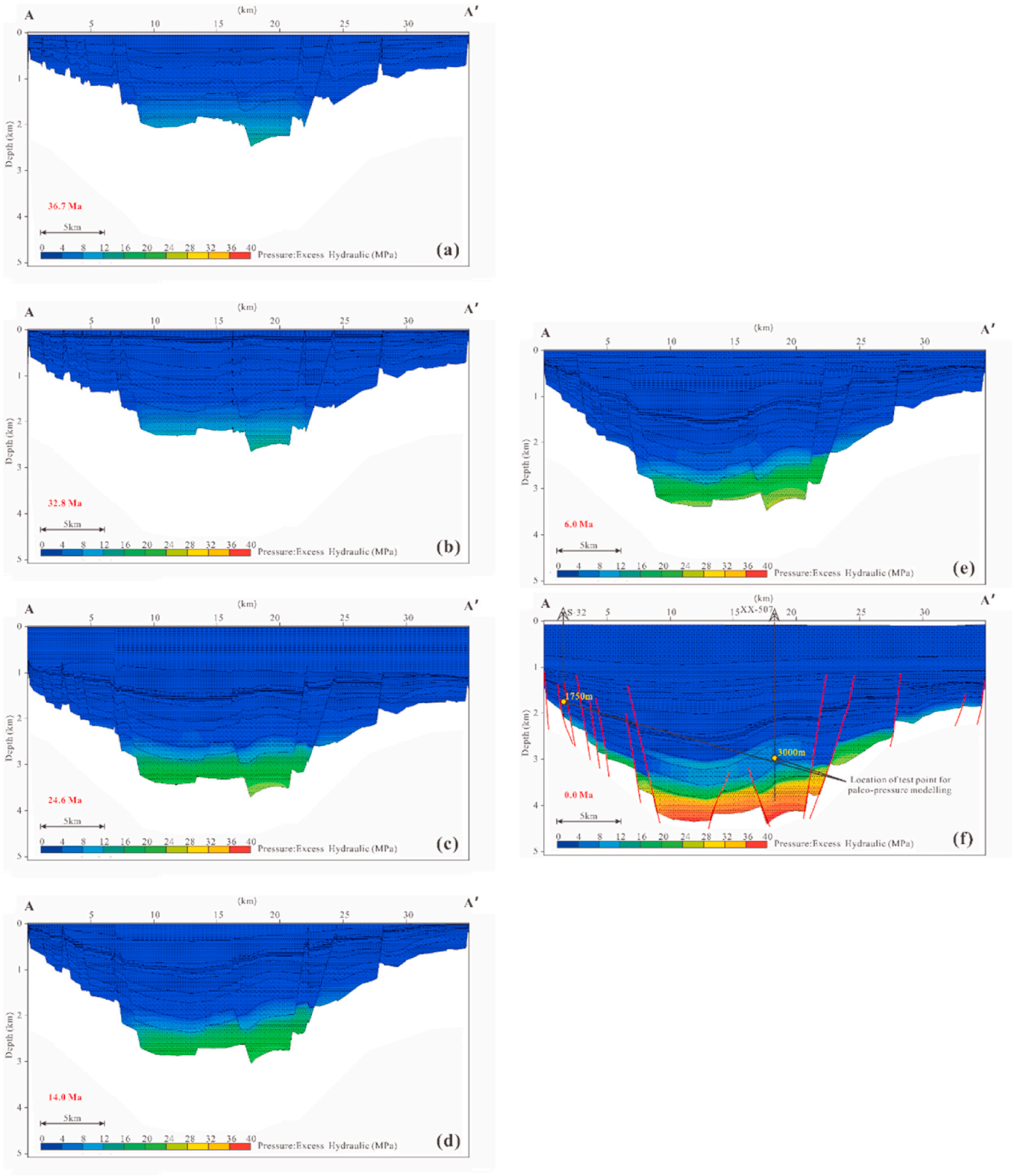

Fig. 17. Evolution of the excess pressure of Section A-A′ obtained by the 2D basin modeling method.

during the tectonic uplift period (24.6–14 Ma) and reached a peak at the end of uplift (Table 8), followed by a gradual decrease and return to normal pressure.

5.3. Matching analysis

5.3.1. Evolution of paleo-pressure by origin analysis

Combined with results of the analysis of the origin of the overpressure and underpressure in the Huimin Depression, a conceptual evolution model of paleo-pressure was established (Fig. 21). In the

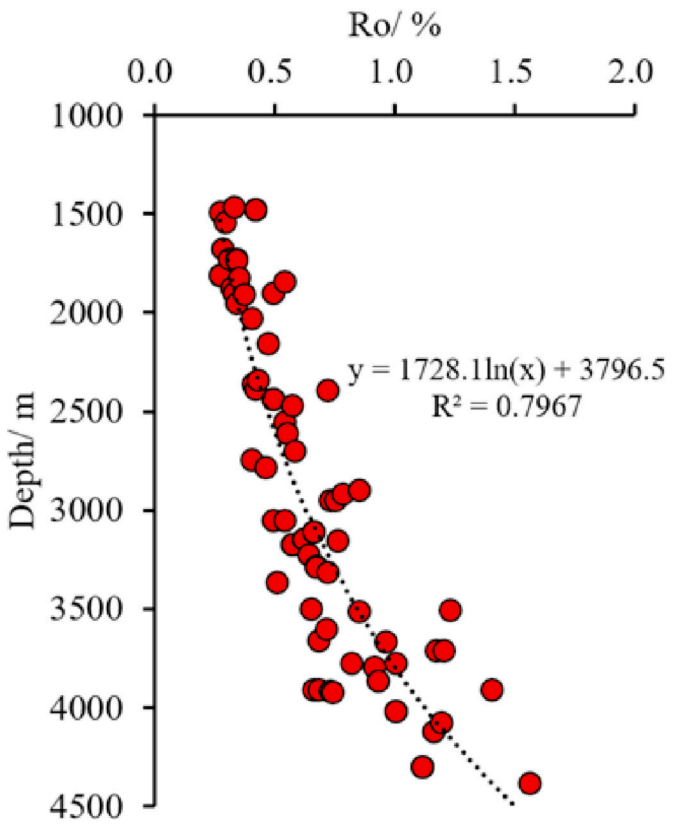

Fig. 18. The relation between the tested and Ro the burial depth.

CDSZ, overpressure occurred and increased to 3.99 MPa during Es_3 before 24.6 Ma. Then, from 24.6 to 14 Ma, tectonic uplift with erosion occurred through the whole depression, which limited the disequilibrium compaction. During this time, elastic rebound of rock and temperature reduction caused underpressure of 1.71 MPa and 0.55 MPa, respectively. With the subsequent deposition from 14 Ma to the present, underpressure due to temperature reduction has been offset. Furthermore, overpressure by disequilibrium compaction and overpressure transformed from hydrocarbon generation from source rocks by hydrocarbon generation increased to 8.88 MPa and 6.39 MPa, respectively. The abnormal pressure in the CDSZ finally is characterized by an overpressure of 13.56 MPa at the present (Fig. 21a).

Hydrocarbon reservoirs in the NTUB were characterized by hydrostatic pressure because of the lack of disequilibrium compaction before 24.6 Ma. From 24.6 to 14 Ma, underpressure caused by elastic rebound of rock and temperature reduction increased to 6.46 and 2.11 MPa, respectively. From 14 Ma to the present, underpressure by temperature reduction has also been offset by subsequent deposition. The abnormal pressure in the NTUB finally is characterized by an underpressure of 6.46 MPa (Fig. 21b). The results of the analysis of the origin show some differences comparing pressure evolution to fluid inclusion methods. The reasons are discussed in the following section.

5.3.2. Matches of paleo-pressure evolution between fluid inclusion method and analysis of origin

The results obtained for paleo-pressure evolution between the results of the reconstruction methods and origin analysis show a good match in both the NTUB and CDSZ, which confirms the reliability and rationality of the results of the reconstruction methods employed in this study (Fig. 22). However, some differences are noted because of difficulty in the quantitative calculation of some geological processes.

(1) In the CDSZ, the pressure evolution by the analysis of the origin was characterized by continuous rise in pressure from 14 Ma to the present. However, pressure evolution by reconstruction methods showed a decreasing process of paleo-Pcoe from 5 Ma to the present. This mismatch may be attributed to the termination of hydrocarbon generation and hydrocarbon migration. Previous studies have shown that the key hydrocarbon generating and accumulating period was from 10 to 3 Ma in the study area (Liu, 2009). On the one hand, the overpressure formed by hydrocarbon generation was not always maintained in the CDSZ. The distributions of the hydrocarbon reservoirs show that hydrocarbon reservoirs are not only distributed in the CDSZ but also in the

Table 6
The evolution of the excess pressure due to the hydrocarbon generation in the Huimin Depression.

Well XX-507				Well S-32			
Time (Ma)	Depth (m)	Ro (%)	$\triangle P_{HG}$* (MPa)	Time (Ma)	Depth (m)	Ro (%)	$\triangle P_{HG}$* (MPa)
38.2	687	0.22	/	38.2	322	0.18	/
36.7	1208	0.29	/	36.7	672	0.22	/
32.8	1462	0.32	/	32.8	736	0.23	/
24.6	2272	0.49	/	24.6	1058	0.27	/
14	2151	0.45	/	14	772	0.23	/
6	2462	0.53	4.51	6	1082	0.27	/
0	4037	1.17	6.39	0	2075	0.44	/

$\triangle P_{HG}$ is the cumulative excess pressure due to hydrocarbon generation.
Parameters of Well XX-507: HI = 220 mg/g, TOC = 2%, and α = 0.85.
Parameters of Well S-32: HI = 178 mg/g, TOC = 1.7%, and α = 0.85.

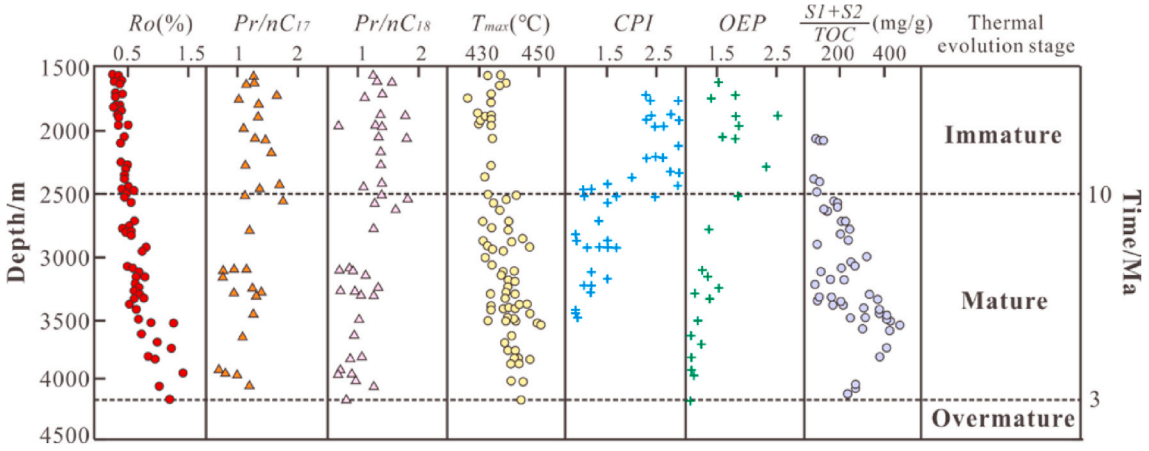

Fig. 19. The relationship between the burial depth and maturity parameters of Es_3 source rock in the Huimin Depression (modified by Zhu and Zeng, 2008).

Table 7
Underpressure values due to rock dilatancy.

Tectonic Zone	Well	ΔZ (m)	ρ_r (g/cm^3)	ΔP_{ER} (MPa)*
NTUB	L-56	646.3	2.36	6.65
	LS-1	602.5	2.34	6.19
	S-13	679.8	2.36	6.99
	S-543	639.7	2.34	6.58
	S-548	574.7	2.26	5.91
	S-69	359.1	2.37	3.69
	S-746	503.8	2.38	5.18
	S-847	522.7	2.38	5.37
	P-9	812.4	2.37	8.35
	PS-3	791.4	2.36	8.14
	PX-5	820	2.36	8.43
Average	/	/	/	6.50
CDSZ	J-202	165.8	2.36	1.71
	J-403	173.1	2.36	1.78
	X-105	177.8	2.38	1.83
	X-510	150.8	2.38	1.55
	X-508	164	2.39	1.69
Average	/	/	/	1.71

ΔZ is the erosional thickness provided by SOB-CPCC, ρ_r is the density of rocks provided by SOB-CPCC, and ΔP_{ER} is the decreased pressure due to elastic rebound.

Table 8
Underpressures by shallow burial depth.

Tectonic Zone	Well	ΔZ (m)	ΔT (°C)	ΔP_{TR} (MPa)*
NTUB	L-56	646.3	22.9	2.15
	LS-1	602.5	21.4	2.01
	S-13	679.8	24.1	2.26
	S-543	639.7	22.7	2.13
	S-548	574.7	20.4	1.91
	S-69	359.1	12.7	1.20
	S-746	503.8	17.9	1.68
	S-847	522.7	18.6	1.74
	P-9	812.4	28.8	2.71
	PS-3	791.4	28.1	2.64
	PX-5	820.0	29.1	2.73
Average	/	/	/	2.11
CDSZ	J-202	165.8	5.9	0.55
	J-403	173.1	6.1	0.58
	X-105	177.8	6.3	0.59
	X-510	150.8	5.4	0.50
	X-508	164.0	5.8	0.55
Average	/	/	/	0.55

ΔZ is the erosional thickness, ΔT is the temperature reduction by a shallow of burial depth, ΔP_{TR} is the decreasing pressure by a shallow burial depth. The paleo-porosity in this calculation is 25.7% according to Zhu et al. (2004)..

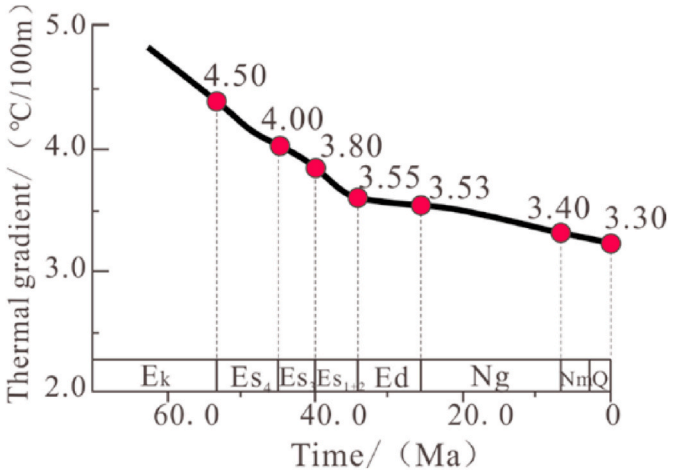

Fig. 20. Evolution of the thermal gradient in the Huimin Depression (Modified by Su et al., 2006).

NTUB (Fig. 1). Therefore, oil and gas also experienced secondary migration in the connected porous sandstone reservoirs from the CDSZ to the NTUB by connected sand bodies and faults (Liu, 2009; Zhu et al., 2010), and hence led to pressure transfer. On the other hand, decreasing of the hydrocarbon generation intensity decreased the overpressured fluids in the Es_3. Combined with the volume loss of pore fluids by hydrocarbon migration and the termination of overpressure supplementation by hydrocarbon generation, the excess pressure in the CDSZ tended to decrease in the late period, which coincided with the paleo-pressure reconstruction results by fluid inclusion method from 5 Ma to the present (Fig. 22a).

(2) In the NTUB, paleo-Pcoe estimated by reconstruction methods show a rising stage followed by a falling stage from 7 Ma to date (Figs. 10b and 22b). However, the analysis of the origin indicated a rising tendency during this stage. This conflict may be attributed to hydrocarbon migration and gas diffusion.

First, as described above, hydrocarbon migration from the CDSZ to the NTUB from 10 to 3 Ma could lead to increases in fluid pressure in the NTUB. Second, gas diffusion is considered to be a substantial reason for locally developed underpressure for loss of mass and hence decreasing of gas volume in pore spaces (Lou et al., 1999; Jin et al., 2004; Yuan and Liu, 2005). Previous studies showed that gas diffusion existed in all hydrocarbon reservoirs and it was intensive on the uplifted tectonic zones and the edge of the basin. The tectonic uplift with erosion often led to an increase in the permeability of the hydrocarbon seals by decreasing the thickness of such seals. Therefore, the sealing capacity of seals decreased (Liu and Xie, 2002). In the Huimin Depression, low-permeable shale or mudstone in the Es_2^2, which is the main seal of the Es_3 reservoirs, shows a thinning tendency of thickness from the CDSZ to the NTUB (Fig. 13). The gas-oil ratios of hydrocarbon reservoirs in the underpressured reservoirs in the NTUB are much lower than those in the adjacent normal-pressured reservoirs and overpressured reservoirs in the CDSZ (Wang et al., 2019). Therefore, the decreasing pressure in the NTUB from approximately 3 Ma to the present might be attributed to gas diffusion, especially for the hydrocarbon accumulating traps in which a large amount of formation water was driven by hydrocarbons (Table 9). However, the decreasing of the pressure in the NTUB from 3Ma to the present needs further research.

5.4. Abnormal pressure evolution model of the Es_3 formation

From the previous analysis, the processes of paleo-pressure evolution are different in the NTUB and the CDSZ. The abnormal pressure evolutionary process of the Es_3 in the Huimin Depression can be divided into 4 stages (Fig. 23).

(1) Early-period compaction stage (32.8 Ma- 24.6 Ma): At this stage, the low-permeable shale and mudstone of the Es_3 in the CDSZ were characterized by weak overpressure by disequilibrium compaction with Pcoe of approximately 1.1–1.2. In the NTUB, abnormal pressure was not developed in the Es_3 owing to relatively low sedimentation rate and hence the shallow burial depth of the strata (Fig. 23a).

(2) Elastic rebound and temperature reduction stage (24.6 Ma- 14.0 Ma): At this stage, the whole depression experienced uplift and erosion. The elastic rebound of rocks due to uplift and erosion caused the pressure to decrease. The erosion of the strata in the NTUB was much more intensive and led to an average pressure decrease of approximately 6.5 MPa. In the CDSZ, the average

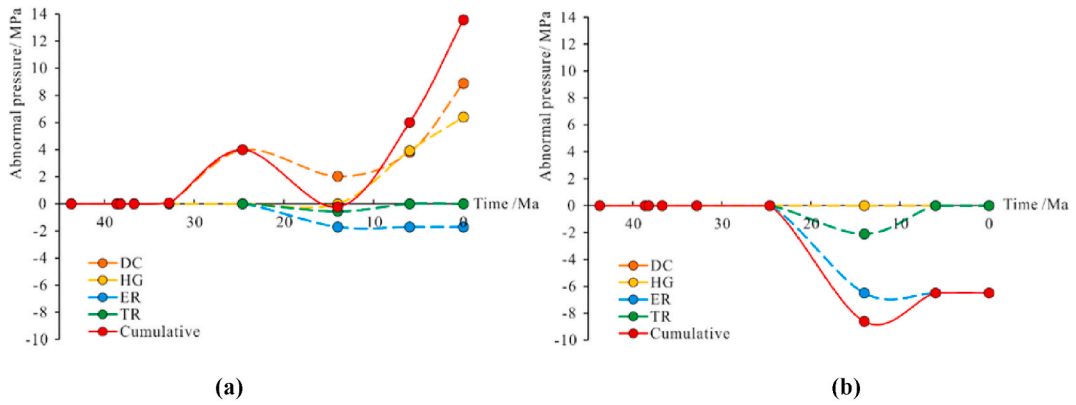

Fig. 21. Evolution of paleo-pressure by origin analysis in (a) the CDSZ and (b) the NUTB. DC = **disequilibrium compaction, HG=hydrocarbon generation, ER=elastic rebound, TR=temperature reduction**.

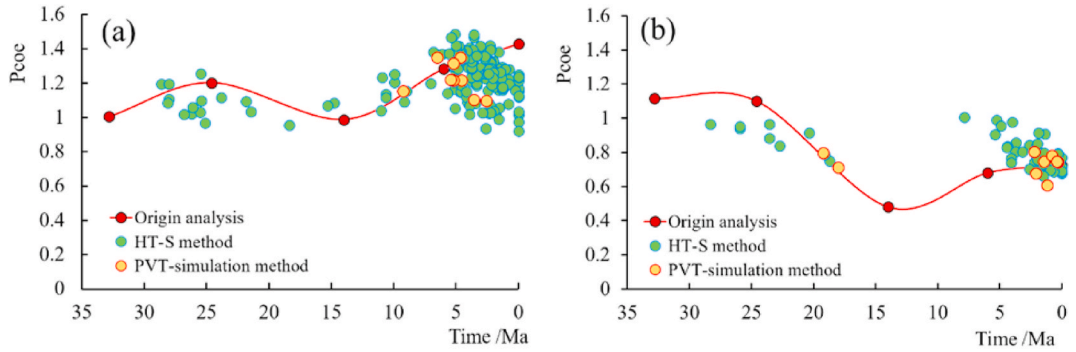

Fig. 22. The match of paleo-pressure evolution between the results of the reconstruction methods and origin analysis of the (a) CDSZ and (b) NTUB.

Table 9
Gas–oil ratio of underpressured reservoirs and adjacent normal-pressured reservoirs (Wang et al., 2019).

Underpressured Reservoir	GOR (m^3/m^3)	Adjacent Normal-Pressured Reservoir	GOR (m^3/m^3)
PX-5	23	P-8	30
P-9	30	P-8	30
T-22	45	P-41	50
S-543	25	S-550	48
S-69	12	S-550	48
S-741	41	S-550	48

pressure decreased due to elastic rebound of rock was approximately 1.7 MPa. Due to the influence of the elastic rebound, the NTUB in this period was characterized by underpressure with Pcoe ranging from 0.6 to 0.8, and the CDSZ in this period was characterized by normal pressure (Fig. 23b).

(3) Late-period compaction, hydrocarbon generation and migration stage (14 Ma- 3 Ma): At this stage, the paleo-pressure increased owing to the late-period subsidence and compaction of the Huimin Depression. Meanwhile, with the increase of burial depth, hydrocarbon generating process started in the CDSZ and led to pressure increases in the Es_3 with Pcoe from 1.4 to 1.5. Furthermore, hydrocarbons generated from the CDSZ migrated to the NTUB and hence led to pressure increasing in the NTUB, which was characterized by normal pressure to weak underpressure (Fig. 23c).

(4) Late-period hydrocarbon migration and gas diffusion stage (3 Ma-0 Ma): At this stage, intensity of hydrocarbon migration gradually weakened owing to the termination of hydrocarbon generation. Therefore, the regional overpressure in the CDSZ decreased to normal pressure or weak overpressure from the central part to the edge with Pcoe ranging from 1.0 to 1.3. Weakening of hydrocarbon migration led to the stop of pressure increasing in the NTUB. Furthermore, gas diffusion through Es_2^1 seals had a poor sealing capacity owing to the thin thickness and erosion of the strata. Finally, weakening of hydrocarbon migration and gas diffusion led to a pressure decrease in the NTUB, which is characterized by underpressure with Pcoe from 0.8 to 0.9 at present (Fig. 23d).

6. Conclusion

(1) The pressure evolution of the CDSZ and the NTUB were different. The CDSZ was characterized by weak overpressure from 32.8 to 24.0 Ma, and then the pressure returned to normal at approximately 14.0 Ma. Strong overpressure developed from 14.0 to 3.0 Ma with Pcoe ranging from 1.2 to 1.5, followed by another decreasing stage from 3.0 Ma to the present with Pcoe ranging from 1.0 to 1.3. The NTUB was characterized by normal pressure at 24.0 Ma. In contrast, underpressure developed during the erosion period, followed by another rising stage from 14 to 3 Ma, during which the pressure had risen to normal. Finally, the NTUB was characterized by underpressure because of the decreasing pressure from 3 Ma to the present.

(2) In the CDSZ, disequilibrium compaction and hydrocarbon generating process led to increasing pressure of 8.88 MPa and 6.39 MPa, respectively. However, overpressure in the NTUB did not develop. In contrast, in the CDSZ, the elastic rebound of rocks and temperature reduction caused decreasing pressure of 1.71 MPa and 0.55 MPa, respectively. In the NTUB, the two factors caused deceasing underpressures of 6.46 MPa and 2.11 MPa, respectively.

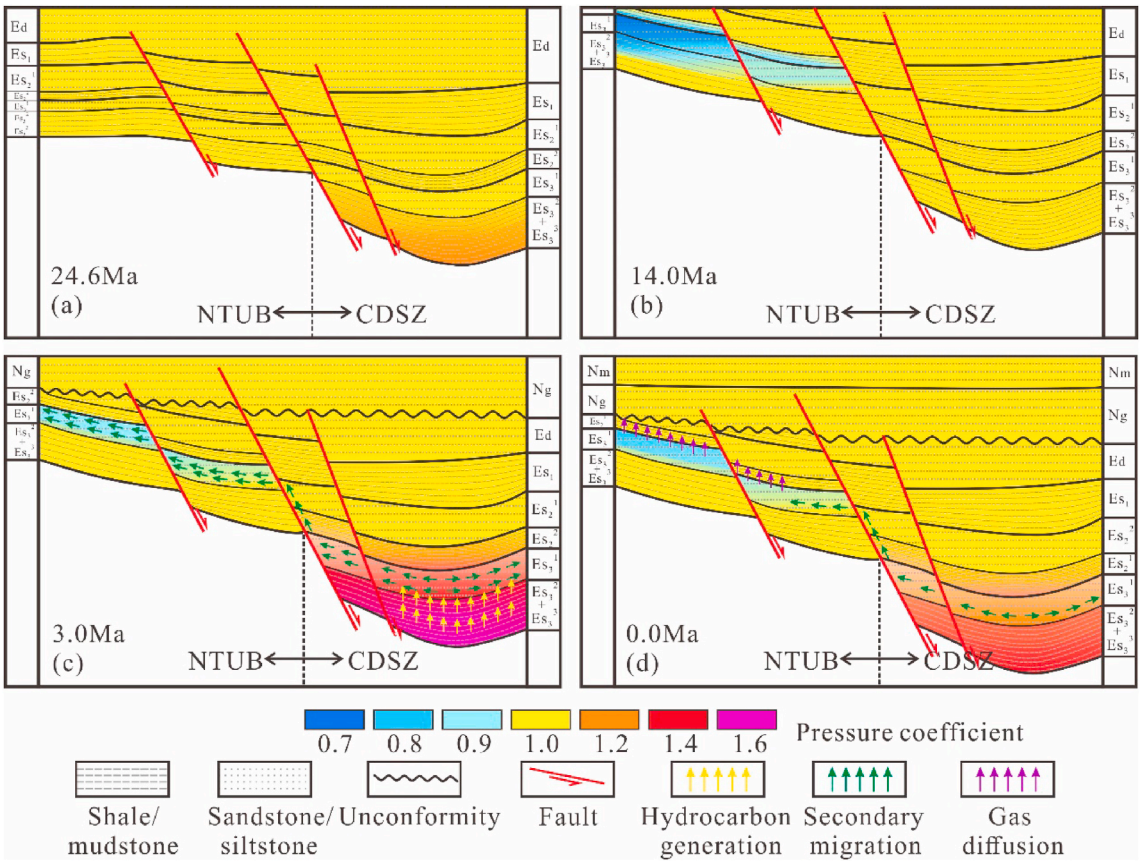

Fig. 23. The abnormal pressure evolution model of the Es_3: (a) Paleo-pressure distribution at 24.6 Ma; (b) Paleo-pressure distribution at 14 Ma; (c) Paleo-pressure distribution at 3 Ma; and (d) Paleo-pressure distribution at 0 Ma.

(3) The evolutionary process of abnormal pressure in the Es_3 could be divided into 4 stages: the early-period compaction stage (32.8–24.6 Ma), elastic rebound and temperature reduction stage (24.6–14 Ma), late-period compaction, hydrocarbon generation and migration stage (14–3 Ma) and late-period secondary migration and gas diffusion stage (3 Ma to the present). The paleo-pressure in the CDSZ had two rising and two falling processes and was finally characterized by the normal pressure or weak overpressure conditions. The paleo-pressure in the NTUB had two falling processes and one rising process without change in the first stage and was finally characterized by underpressure.

Credit author statement

Qiaochu Wang: Formal analysis, investigation, writing-original draft, writing- review & editing. Dongxia Chen: Supervision, conceptualization, methodology. Xianzhi Gao: Methodology, software. Fuwei Wang: Data curation, writing- review & editing. Sha Li: Formal analysis. Ziye Tian: Data curation, validation. Wenzhi Lei: Investigation. Siyuan Chang: Writing- review & editing. Yi Zou: Data curation.

Declaration of competing interest

The authors declare that they have no known competing financial interests or personal relationships that could have appeared to influence the work reported in this paper.

Acknowledgements

This work was supported by the National Natural Science Foundation of China (Grant No. 41972124). We are very grateful to the Beijing Research Institute of Uranium Geology for sample analysis and experiments. We also thank the Shengli Oilfield Branch of the China Petroleum and Chemical Corporation for providing geological information and test data for this study.

Appendix A. Supplementary data

Supplementary data to this article can be found online at https://doi.org/10.1016/j.petrol.2021.108601.

References

Abdel-Fattah, M.I., Pigott, J.D., Abd-Allah, Z.M., 2017. Integrative 1D-2D basin modeling of the cretaceous Beni Suef basin, western Desert, Egypt. J. Petrol. Sci. Eng. 153, 297–313.

Abdelwahhab, A.M., Reaf, A., 2020. Integrated reservoir and basin modeling in understanding the petroleum system and evaluating prospects: the cenomanian reservoir, Bahariya formation, at Falak field, Shushan basin, western Desert, Egypt. J. Petrol. Sci. Eng. 189 https://doi.org/10.1016/j.petrol.2020.107023.

Al-Khafaji, J.A., Hakimi, H.M., Mohialdeen, J.M.I., Idan, M.R., Afify, E.W., Lashin, A.A., 2021. Geochemical characteristics of crude oils and basin modelling of the probable source rocks in the Southern Mesopotamian Basin, South Iraq. J. Petrol. Sci. Eng. 196 https://doi.org/10.1016/j.petrol.2020.107641.

Amyx, J.W., Bass, D.M., Whiting, R.L., 1960. Petroleum Reservoir Engineering, Physical Properties. McGraw-Hill, New York, p. 610.

Aplin, A.C., Macleod, G., Larter, S.R., Pedersen, K.S., Sorensen, H., Booth, T., 1999. Combined use of Confocal Laser Scanning Microscopy and PVT simulation for estimating the composition and physical properties of petroleum in fluid inclusions. Mar. Petrol. Geol. 16 (2), 97–110.

Baker, C., 1972. Aquathermal pressuring-role of temperature in the development of abnormal pressure zones. AAPG (Am. Assoc. Pet. Geol.) Bull. 56 (10), 2068–2871.

Bakker, R.J., 2018. AqSo_NaCl: computer program to calculate p-T-V-x properties in the H_2O-NaCl fluid system applied to fluid inclusion research and pore fluid calculation. Comput. Geosci. 115, 122–133.

Bakker, R.J., Doppler, G., 2016. Salinity and density modifications of synthetic H_2O and H_2O–NaCl fluid inclusions in re-equilibration experiments at constant temperature and confining pressure. Chem. Geol. 424, 73–85.

Bodnar, R.J., Sterner, S.M., 1987. Synthetic fluid inclusions. In: Barnes, H.L., Ulmer, G.C. (Eds.), Hydrothermal Experimental Techniques. Wiley, New York, pp. 423–457.
Bourdet, J., Pironon, J., Levresse, G., Tritlla, J., 2010. Petroleum accumulation and leakage in a deeply buried carbonate reservoir, Níspero field (Mexico). Mar. Petrol. Geol. 27, 126–142.
Bowers, T.S., Helgeson, H.C., 1983. Calculation of the thermodynamic and geochemical consequences of non-ideal mixing in the system H_2O-CO_2-NaCl on phase relations in geological systems: equation of state for H_2O-CO_2-NaCl fluids at high pressures and temperatures. Geochem. Cosmochim. Acta 47, 1247–1275.
Bredehoeft, J.D., Wesley, J.B., Fouch, T.D., 1994. Simulations of the origin of fluid pressure, fracture generation, and movement of fluids in the Uinta basin, Utah. AAPG (Am. Assoc. Pet. Geol.) Bull. 78, 1729–1747.
Burnham, A.K., Braun, R.L., Gregg, H.R., Samoun, A.M., 1987. Comparison of methods for measuring kerogen pyrolysis rates and fitting kinetic parameters. Journal of Energy & Fuels 1, 452–458.
Burrus, J., 1998. Overpressure models for clastic rocks, their relation to hydrocarbon expulsion: a critical reevaluation. AAPG Memoir 70, 35–63.
Caillet, G., Judge, N.C., Bramwell, N.P., Meciani, L., Green, M., Adam, P., 1997. Overpressure and hydrocarbon trapping in the chalk of the Norwegian central Graben. Petrol. Geosci. 3 (1), 33–42.
Carvajal-Arenas, C.L., Torrado, L., Mann, P., English, J., 2020. basin modeling of late cretaceous/Mio-Pliocene (.) petroleum system of the deep-water eastern Colombian basin and south caribbean Deformed belt. Mar. Petrol. Geol. 121 https://doi.org/10.1016/j.marpetgeo.2020.104511.
Corbet, T.F., Bethke, C.M., 1992. Disequilibrium fluid pressures and groundwater flow in the Western Canada sedimentary basin. J. Geophys. Res. 97 (B5), 7203–7217.
Ding, Z.Y., Wang, L.S., Hu, W.X., Zhang, P., Liu, S.W., Mi, N., 2008. Reconstruction of Cenozoic thermal history of Bohai Bay Basin with a transient heat flow model. Acta Pet. Sin. 29 (5), 650–656.
Driesner, T., Heinrich, C.A., 2007. The system H_2O-NaCl. Part I. Correlation formulae for phase relations in temperature-pressure-composition space from 0 to 1000 °C, 0 to 5000 bar, and 0 to 1 X_{NaCl}. Geochem. Cosmochim. Acta 71, 4880–4901.
DuBow, J., 1984. Temperature effects. In: Chong, K.P., Smith, J.W. (Eds.), Mechanics of Oil Shale. Elsevier Applied Science Publishers, London, pp. 523–577.
Durand, B., 1983. Present trends in organic geochemistry in research on migration of hydrocarbons. In: Advances in Organic Chemistry. John Wiley, New York, pp. 117–128.
Eaton, B.A., 1975. The Equation for Geopressure Prediction from Well Logs. Society of Petroleum Engineers of AIME. Paper SPE 5544.
Falvey, D.A., Middleton, M.F., 1981. Passive continental margins: evidence for a prebreakup deep crustal metamorphic subsidence mechanism. Oceanol. Acta 4 (Suppl. l), 103–114.
Fatt, I., 1958. Compressibility of sandstones at low to moderate pressure. AAPG (Am. Assoc. Pet. Geol.) Bull. 42 (12), 1924–1957.
Feng, D.X., 2010. Comprehensive evaluation of lower Sha3 reservoir in south Linnan Depression. Petroleum geology and recovery efficiency 17 (1), 33–36.
Gac, S., Hansford, P.A., Faleide, J.I., 2018. Basin modelling of the SW Barents Sea. Mar. Petrol. Geol. 95, 167–187.
Goldstein, R.H., Reynolds, T.J., 1994. Systematics of fluid inclusions in diagenetic minerals. Society for Sedimentary Geology Short Course 31, 199.
Guo, X.L., Xiong, M., Zhou, T., Tian, H., Xiao, X.M., 2009. Petroleum generation and expultion kinetics: a case study of the Shahejie Formation source rocks from Linnan Sag of Huimin Depression. Acta Sedmentologica Sinica 27 (4), 723–731.
Guo, X.W., He, S., Liu, K.Y., Song, G.Q., Wang, X.J., Shi, Z.S., 2010. Oil generation as the dominant overpressure mechanism in the cenozoic Dongying depression, Bohai Bay Basin, China. AAPG (Am. Assoc. Pet. Geol.) Bull. 94, 1859–1881.
Guo, X.W., He, S., Liu, K.Y., Zheng, L.J., 2011a. Quantitative estimation of overpressure caused by oil generation in petroliferous basins. Org. Geochem. 42, 1343–1350.
Guo, X.W., He, S., Song, G.Q., Wang, X.J., Wang, B.J., Li, N., Luo, S.Y., 2011b. Evidences of overpressure caused by oil generation in Dongying Depression. Earth Sci. J. China Univ. Geosci. 36 (6), 1085–1094.
Hakimi, H.M., Alaug, A.S., Mohialdeen, I.M.J., Kahal, A.Y., Abdulelah, H., Hadad, Y.T., Yahya, M.M.A., 2019. Late Jurassic Arwa Member in south-eastern Al-Jawf sub-basin, NW Sabatayn Basin of Yemen: geochemistry and basin modeling reveal shale-gas potential. J. Nat. Gas Sci. Eng. 64, 133–151.
Hakimi, H.M., Najaf, A.A., Abdula, A.R., Mohiadeen, J.M.I., 2018. Generation and expulsion history of oil-source rock (Middle Jurassic Sargelu Formation) in the Kurdistan of north Iraq, Zagros folded belt: implications from 1D basin modeling study. J. Petrol. Sci. Eng. 162, 852–872.
Hantschel, T., Kauerauf, A., et al., 2009. Fundamentals of Basin and Petroleum Systems Modeling. Springer, Germany.
Hao, F., 2005. Kinetics of Hydrocarbon generation and mechanisms of petroleum accumulation in overpressured basins. Science Press, Beijing.
Hedberg, H.H., 1974. Relation of methane generation to undercompacted shales, shale diapirs, and mud volcanoes. AAPG (Am. Assoc. Pet. Geol.) Bull. 58, 661–673.
Heppard, P.D., Cander, H.S., Eggertson, E.B., 1998. Abnormal Pressure and the Occurrence of Hydrocarbons in Offshore Eastern Trinidad, West Indies, vol. 70. AAPG Memoir, pp. 215–246.
Hodgman, C.D., 1957. Handbook of Chemistry and Physics. Chemical Rubber Pub Co., Cleveland, Ohio, p. 3213.
Huang, Y.T., Yao, G.Q., Zhou, F.D., Wang, T.T., 2017. Impact factors on reservoir quality of clastic Huangliu formation in overpressure diapir zone, Yinggehai Basin, China. J. Petrol. Sci. Eng. 154 (6), 322–336.
Jawad, A., Saleh, M., Hassan, O.F., 2012. Comprehensive model for flash calculations of heavy oils using the Soave-Redlich-Kwong equation of state. In: North Africa Technical Conference and Exhibition.
Jin, B., Liu, Z., Zhang, R.X., Guo, F., 2004. The anomalous low pressure (negative pressure) and hydrocarbon accumulation in a sedimentary basin. Acta Geoscientica Sinica 25 (3), 351–356.
Karlsen, D., Nedkvitne, T., Larter, S.R., Bjorlykke, K., 1993. Hydrocarbon composition of authigenic inclusions: applications to elucidation of petroleum reservoir filling history. Geochem. Cosmochim. Acta 57, 3641–3659.
Lash, G.G., Englender, T., 2005. An analysis of horizonal microcracking during catagenesis: example from the Catskill delta complex. AAPG (Am. Assoc. Pet. Geol.) Bull. 89 (11), 1433–1449.
Law, B.E., Bostick, N.H., 1980. Evaluation of organic matter, subsurface temperature and pressure with regards to gas generation in low-permeability Upper Cretaceous and lower Tertiary sandstones in Pacific Creek area, Sublette and Sweetwater Counties. Wyoming: Mt. Geol. 17, 23–35.
Law, B.E., Dickinson, W.W., 1985. Conceptual-model for origin of abnormally pressured gas accumulation in low-permeability reservoirs. AAPG (Am. Assoc. Pet. Geol.) Bull. 69 (8), 1295–1304.
Law, B.E., Spencer, C.W., 1998. Abnormal pressure in hydrocarbon environments. AAPG Memoir 70, 1–11.
Li, J., Zhao, J.Z., Wei, X.S., Chen, M.N., Song, P., Han, Z.H., Wu, W.T., 2019. Origin of abnormal pressure in the upper Paleozoic shale of the ordos basin, China. Mar. Petrol. Geol. 110 (12), 62–177.
Li, C.Q., Liu, H.M., 2013. Abnormal formation pressure and its evolution features of the third member, Shahejie Formation, Linnan sag. Earth Sci. J. China Univ. Geosci. 38 (1), 105–111.
Li, Q., Jiang, Z.X., Liu, K.Y., Zhang, C.M., You, X.L., 2014. Factors controlling reservoir properties and hydrocarbon accumulation of lacustrine deep-water turbidites in the Huimin Depression, Bohai Bay Basin, East China. Mar. Petrol. Geol. 57, 327–344.
Li, S.X., Shi, Z.J., Liu, X.Y., Yang, S.Y., Deng, X.Q., Liu, G.L., Li, J.H., 2013. Quantitative analysis of the Mesozoic abnormal low pressure in Ordos Basin. Petrol. Explor. Dev. 40 (5), 528–533.
Li, X.L., He, Y.B., Wang, N., Xing, Y., Zhang, X., 2018. Reservoir characteristics and controlling factors of the second member of Dongying formation in Dalujia area, Huimin Depression. China Science Paper 13 (9), 1002–1011.
Liu, D.H., Xiao, X.M., Mi, J.K., Li, X.Q., Shen, J.K., Song, Z.G., Peng, P.A., 2003. Determination of trapping pressure and temperature of petroleum inclusions using using PVT simulation software-a case study of Lower Ordovician carbonates from the Lunnan Low Uplift, Tarim Basin. Mar. Petrol. Geol. (20), 29–43.
Liu, H., Jiang, Y.L., Lu, H., Liu, Y.L., Jing, C., 2016a. Restoration of fluid pressure during hydrocarbon accumulation period and fluid inclusion feature in the Bonan Sag. Earth Sci. 41 (8), 1384–1394.
Liu, H., Jiang, Y.L., Song, G.Q., Cai, D.M., Xu, H.Q., 2012. Pressure evolution and gas accumulation of the fourth member of the Shahejie Formation in Dongying depression, Bohai Bay Basin. Acta Sedimentol. Sin. 30 (1), 198–203.
Liu, H., Jiang, Y.L., Song, G.Q., Gu, G.C., Hao, L., Feng, Y.L., 2017. Overpressure characteristics and effects on hydrocarbon distribution in the Bonan sag, Bohai Bay Basin, China. Journal of Petroleum and Engineering 149, 811–821.
Liu, H.M., 2009. Hydrocarbon migration and accumulation direction and distribution of Linnan sag in Jiyang depression. Geoscience 23 (5), 894–901.
Liu, H.P., Bi, X.W., Lu, H.Z., Hu, R.Z., Lan, T.G., Wang, X.S., Huang, M.L., 2018a. Nature and evolution of fluid inclusions in the Cenozoic Beiya gold deposit, SW China. J. Asian Earth Sci. 161, 35–56.
Liu, J.D., Liu, T., Jiang, Y.L., Wan, T., Liu, R.N., 2019. Distribution, origin, and evolution of overpressure in the Shahejie Formation of northern Dongpu depression, Bohai Bay Basin, China. J. Petrol. Sci. Eng. 181 https://doi.org/10.1016/j.petrol.2019.106219.
Liu, Q.Y., He, L.J., 2019. Tectono-thermal modeling of the Bohai Bay Basin since the cenozoic. Chin. J. Geophys. 62 (1), 219–235.
Liu, X.F., 2011. Distribution and origin of the abnormal pressure in a transitional basin: a case study from Linnan Subsag, Huimin Sag. Geol. Sci. Technol. Inf. 30 (5), 1–11.
Liu, X.F., Xie, X.N., 2002. Origin and characteristics of under pressure systems in Dongying Depression. Oil Gas Geol. 23 (1), 66–69.
Liu, Y.F., Qiu, N.S., Xie, Z.Y., Yao, Q.Y., Chuan, Q.Z., 2016b. Overpressure compartments in the central paleo-uplift, Sichuan basin, southwest China. AAPG (Am. Assoc. Pet. Geol.) Bull. 100, 867–888.
Liu, Y.F., Qiu, N.S., Yao, Q.Y., Chang, J., Xie, Z.Y., 2016c. Distribution, origin and evolution of the upper Triassic overpressures in the central portion of the Sichuan basin, SW China. J. Petrol. Sci. Eng. 146, 1116–1129.
Liu, Y.Q., Zeng, J.H., Zhou, L., 2018b. Geochemical characteristics and origin of Shahejie Formation water in Huimin sag. Geoscience 27 (5), 1110–1119.
Liu, Y.Q., Zeng, J.H., Zhou, L., Zhai, S.J., 2013. Geochemical characteristics and origin of Shahejie Formation water in Huimin sag. Geoscience 27 (5), 1110–1119.
Lou, Z.H., Gao, R.Q., Cai, X.Y., Xu, H., 1999. The evolution of fluid dynamic field and the origin of subnormal pressure in Songliao Basin, China. Acta Pet. Sin. 20 (6), 27–31.
Luo, X., Vasseur, G., 1995. Modelling of pore pressure evolution associated with sedimentation and uplift in sedimentary basins. Basin Res. 7 (1), 35–52.
Macleod, G., Larter, S.R., Aplin, A.C., Petch, G.S., 1994. Improved analysis of petroleum fluid inclusions: application to reservoir studies. Abstracts of The American Chemical Society 207, 132.
Magara, K., 1975. Reevaluation of montmorillonite dehydration as cause of abnormal pressure and hydrocarbon migration. AAPG (Am. Assoc. Pet. Geol.) Bull. 59, 292–302.
Marine, I.W., Fritz, S.J., 1981. Osmotic model to explain anomalous hydraulic heads. Water Resour. Res. 17, 73–82.
Masters, J.A., 1979. Deep basin gas trap, western Canada. AAPG (Am. Assoc. Pet. Geol.) Bull. 63 (2), 152–181.
McCain, W.D., 2017. The Properties of Petroleum Fluids, p. 248. Tulsa, Oklahoma, PennWell.

Meissner, F.F., 1978. Petroleum geology of the Bakken formation, Williston basin, north Dakota and Montana. In: 24th Annual Conference, Williston Basin Symposium. Montana Geological Society, pp. 207–227.
Mi, J.Q., Xiao, X.M., Liu, D.H., Shen, J.G., 2002. Simulation for minimum trapping pressure of inclusions occurring in Upper Paleozoic sandstone reservoir of Ordos Basin using PVTsim. Geochimica 31 (4), 402–406.
Mouchet, J.P., Mitchell, A., 1989. Abnormal pressures while drilling. Manuels Tech. Elf Aquitaine 2, 264.
Moernaut, J., Wiemer, G., Reusch, A., Stark, N., Batist, M.D., Urrutia, R., Guevara, B.L., Kopf, A., Strasser, M., 2017. The influence of overpressure and focused fluid flow on subaquatic slope stability in a formerly glaciated basin: Lake Villarrica (South-Central Chile). Mar. Geol. 383 (1), 35–54.
Neuzil, C.E., 2000. Osmotic generation of 'anomalous' fluid pressures in geological environments. Nature 403, 182–184.
Nishiyama, N., Sumino, H., Ujiie, K., 2020. Fluid overpressure in subduction plate boundary caused by mantle-derived fluids. Earth Planet Sci. Lett. 538 https://doi.org/10.1016/j.epsl.2020.116199.
Oloruntobi, O., Adedigba, S., Khan, F., Chunduru, R., Butt, S., 2018. Overpressure prediction using the hydro-rotary specific energy concept. J. Nat. Gas Sci. Eng. 55 (6), 243–253.
Peng, B., Hao, F., Zou, H.Y., 2013. Development and evolution of overpressure and episodic hydrocarbon accumulation in northern Liaozhong Subdepression of Liaodong bay area. Geol. Rev. 59 (6), 1257–1267.
Peng, B., Zou, H.Y., 2013. Present-day geothermal structure of lithosphere and the Cenozoic tectono-thermal evolution of Bohai Basin. Geoscience 27 (6), 1399–1406.
Qiu, N.S., Su, X.G., Li, Z.Y., Liu, Z.Q., Li, Z., 2006. The cenozoic tectono-thermal of Jiyang depression, Bohai Bay Basin, east China. Chinese Journal of Geophisics 49 (4), 1127–1135.
Reeves, S.R., Kuuskraa, V.A., Hill, D.G., 1996. New basins invigorate U.S. gas shales play. Oil Gas J. 22 (1), 53–58.
Roberts, S.J., Nunn, J.A., 1995. Episodic fluid expulsion from geopressured sediments. Mar. Petrol. Geol. 12, 195–204.
Roedder, E., 1984. Fluid Inclusions. Reviews in Mineralogy, vol. 12. American Mineralogical Society, p. 644.
Russell, W.L., 1972. Pressure-depth relations in Appalachian region. AAPG (Am. Assoc. Pet. Geol.) Bull. 56 (3), 528–536.
Stefan, B., Underschultz, J.R., 1995. Large-scale underpressuring in Mississippian-cretaceous Succession, southwestern alberta basin. AAPG (Am. Assoc. Pet. Geol.) Bull. 79 (7), 989–1004.
Su, X.G., Qiu, N.S., Liu, Z.Q., 2006. An analysis of thermal evolution history of Huimin sag in Jiyang depression. Nat. Gas. Ind. 26 (10), 15–17.
Sun, Y., Zhong, J.H., Yuan, X.C., Jiang, Z.X., Yang, W.L., Li, S.Y., 2008. Analysis on sequence stratigraphy of lacustrine carbonate in the first member of Shahejie Formation in Huimin Sag. Acta Pet. Sin. 29 (2), 213–218.
Swarbrick, R.E., Osborne, M.J., 1998. Mechanisms that generate abnormal pressures: an overview. AAPG Memoir 70, 13–34.
Swarbrick, R.E., Osborne, M.J., Grunberger, D., Yardley, G.S., Macleod, G., Aplin, A.C., Larter, S.R., Knight, I., Auld, H.A., 2000. Integrated study of the Judy field (Block 30/7a) –an overpressured central north Sea oil/gas field. Mar. Petrol. Geol. 17, 993–1010.
Sweeney, J.J., Burnham, A.K., 1990. Evaluation of a simple model of vitrinite reflectance based on chemical kinetics. AAPG (Am. Assoc. Pet. Geol.) Bull. 74, 1559–1570.
Tang, Y., Stauffer, M., 1994. Multiple cold trap pyrolysis gas chromatography: a new technique for modeling hydrocarbon generation. Org. Geochem. 22 (3–5), 0-872.
Teinturier, S., Pironon, J., Walgenwitz, F., 2002. Fluid inclusions and PVTX modelling: examples from the Garn formation in well 6507/2-2, Haltenbanken, Mid-Norway. Mar. Petrol. Geol. 19, 755–765.
Tingay, M.R.P., Hillis, R.R., Swarbrick, R.E., Morley, C.K., Damit, A.R., 2009. Origin of overpressure and pore-pressure prediction in the Baram province, Brunei. AAPG (Am. Assoc. Pet. Geol.) Bull. 93 (1), 51–74.
Wang, B., Zhang, L.K., Li, C., Chen, K.Y., Song, G.Q., Luo, H.M., 2018. Mechanism and distribution prediction of abnormal high pressure of the Paleocene Shahejie Formation in Linnan sag, Huimin depression. Oil Gas Geol. 39 (4), 641–652.
Wang, Q.C., Chen, D.X., Wang, F.W., Li, J.H., Liao, W.H., Wang, Z.Y., Xie, G.J., Shi, X.B., 2019. Underpressure characteristics and origins in the deep strata of rift basins: a case study of the Huimin Depression, Bohai Bay Bain, China. Geol. J. https://doi.org/10.1002/gj.3651.
Wygrala, B.P., 1989. Integrated Study of an Oil Field in the Southern Po Basin, Northern Italy. Forschungszentrums Karlsruhe Juelich, p. 217.
Xie, R.H., Zhou, W., Yang, Z.B., 2003. Testing characteristics and log interpretation of rock's Poission ratio under simulating formation condition. Well Logging Technol. 35 (3), 218–223.
Xie, W., Nie, F.J., Zhang, S.P., Liu, C.D., Wang, W.Q., Xia, F., Yan, Z.B., Zhang, C.Y., 2009. Thermal evolution modeling of hydrocarbon fluids n the Dongying Depression based on Basin-2 software. Acta Geol. Sichuan 29 (4), 481–483.
Yang, Y., Aplin, A.C., Larter, S.R., 2004. Quantitative assessment of mudstone lithology using geophysical wireline logs and artificial neural networks. Petrol. Geosci. 10 (2), 141–151.
Yielding, G., Freeman, B.D., Needham, T., et al., 1997. Quantitative fault seal prediction. AAPG Bull. 81 (6), 897–917.
Yuan, J.H., Liu, G.D., 2005. Distribution characteristics and formation processes of Upper Paleozoic abnormally low pressure zones in Ordos Basin. Oil Gas Geol. 26 (6), 792–799.
Zhang, J., 2013. Effective stress, porosity, velocity and abnormal pore pressure prediction accounting for compaction disequilibrium and unloading. Mar. Petrol. Geol. 45, 2–11.
Zhang, J.C., 2019. Applied Petroleum Geomechanics. Gulf Professional Publishing, pp. 233–280.
Zhang, Y.G., Frantz, J.D., 1987. Determination of the homogenization temperature and densities of supercritical fluids in the system NaCl-KCl-$CaCl_2$-H_2O using synthetic fluid inclusions. Chem. Geol. 64, 335–350.
Zhao, Y., Liu, Z., Dai, L.C., 2004. The analysis of the characteristics of subnormal pressure and hydrocarbon accumulation in Linnan Subsag, Huimin Sag. J. NW Univ. 34 (6), 713–716.
Zhu, X.M., Zhong, D.K., Zhang, Q., Zhang, L., 2004. Sandstone Diagenesis and porosity evolution of Paleogene in Huimin depression. Petrol. Sci. 1 (3), 23–29.
Zhu, Z.Q., Zeng, J.H., 2008. Feature of fluid inclusions and the period of petroleum accumulation in Linnan Sag. Journal of Southwest Petroleum University (Science and Technology Edition) 30 (4), 31–34.
Zhu, Z.Q., Zeng, J.H., Wang, J.J., 2010. Hydrocarbon migration characteristics of Linnan sag in Huimin depression. Journal of Southwest Petroleum University (Science & Technology Edition) 32 (4), 32–38.